

# Permian–Triassic boundary microbialites (PTBMs) in southwest China: implications for paleoenvironment reconstruction

Hao Tang<sup>1,3</sup> · Stephen Kershaw<sup>2</sup> · Hong Liu<sup>1,3</sup> · Xiucheng Tan<sup>1,3</sup> · Fei Li<sup>1,3</sup> ·  
Guang Hu<sup>1,3</sup> · Cheng Huang<sup>1,3</sup> · Lichao Wang<sup>1,3</sup> · Chengbo Lian<sup>1,3</sup> · Ling Li<sup>1,3</sup> ·  
Xuefei Yang<sup>1,3</sup>

Received: 26 April 2016 / Accepted: 26 September 2016 / Published online: 8 November 2016  
© The Author(s) 2016. This article is published with open access at Springerlink.com

**Abstract** Permian–Triassic boundary microbialites (PTBMs) are commonly interpreted to be a sedimentary response to upwelling of anoxic alkaline seawater and indicate a harsh marine environment in the Permian–Triassic transition. However, recent studies propose that PTBMs may instead be developed in an oxic environment, therefore necessitating the need to reassess the paleoenvironment of formation of PTBMs. This paper is an integrated study of the PTBM sequence at Yudongzi, northwest Sichuan Basin, which is one of the thickest units of PTBMs in south China. Analysis of conodont biostratigraphy, mega- to microscopic microbialite structures, stratigraphic variations in abundance and size of metazoan fossils, and total organic carbon (TOC) and total sulfur (TS) contents within the PTBM reveals the following results: (1) the microbialites occur mainly in the *Hindeodus parvus* Zone but may cross the Permian–Triassic boundary, and are comprised of, from bottom to top: lamellar thrombolites, dendritic thrombolites and lamellar-reticular thrombolites; (2) most metazoan fossils of the microbialite succession increase in abundance upsection, so does the sizes of bivalve and brachiopod fossils; (3) TOC and TS values of microbialites account respectively for 0.07 and 0.31 wt% on average, both of which are very low. The

combination of increase in abundance and size of metazoan fossils upsection, together with the low TOC and TS contents, is evidence that the Yudongzi PTBMs developed in oxic seawater. We thus dispute the previous view, at least for the Chinese sequences, of low-oxygen seawater for microbialite growth, and question whether it is now appropriate to associate PTBMs with anoxic, harsh environments associated with the end-Permian extinction. Instead, we interpret those conditions as fully oxygenated.

**Keywords** Permian–Triassic boundary microbialites (PTBMs) · Conodont · Anoxic upwelling · Redox condition · Early Triassic recovery · Yudongzi · Southwest China

## Introduction

The end-Permian mass extinction, which caused the extinction of more than 90% of marine invertebrate species, not only significantly changed Late Permian ecosystems but also dramatically influenced sedimentary systems, resulting in the widespread presence of unusual deposits that are commonly referred to as anachronistic facies (coined by Sepkoski et al. 1991), such as flat pebble conglomerates, subtidal wrinkle structures, vermicular limestone, microbialites, and carbonate seafloor aragonite fans (Zhao et al. 2008; Woods 2014 and references therein). Among all these, microbialites that crossed the Permian–Triassic boundary (and thus here called Permian–Triassic boundary microbialites, PTBMs) have been intensively studied because of the evidence they provide on the nature of the latest Permian mass extinction and its aftermath (Kershaw et al. 1999, 2002; Lehrmann 1999; Lehrmann et al. 2003; Ezaki et al. 2003, Wang et al. 2005; Wu et al. 2007; Ezaki

✉ Hong Liu  
thufocom@163.com

<sup>1</sup> State Key Laboratory of Oil and Gas Reservoir Geology and Exploitation, Southwest Petroleum University, Chengdu 610500, China

<sup>2</sup> Department of Life Sciences, Brunel University, Kingston Lane, Uxbridge UB8 3PH, UK

<sup>3</sup> Key Laboratory of Carbonate Reservoir of CNPC, Department of Sedimentology and Hydrocarbon Accumulation, Southwest Petroleum University, Chengdu 610500, China

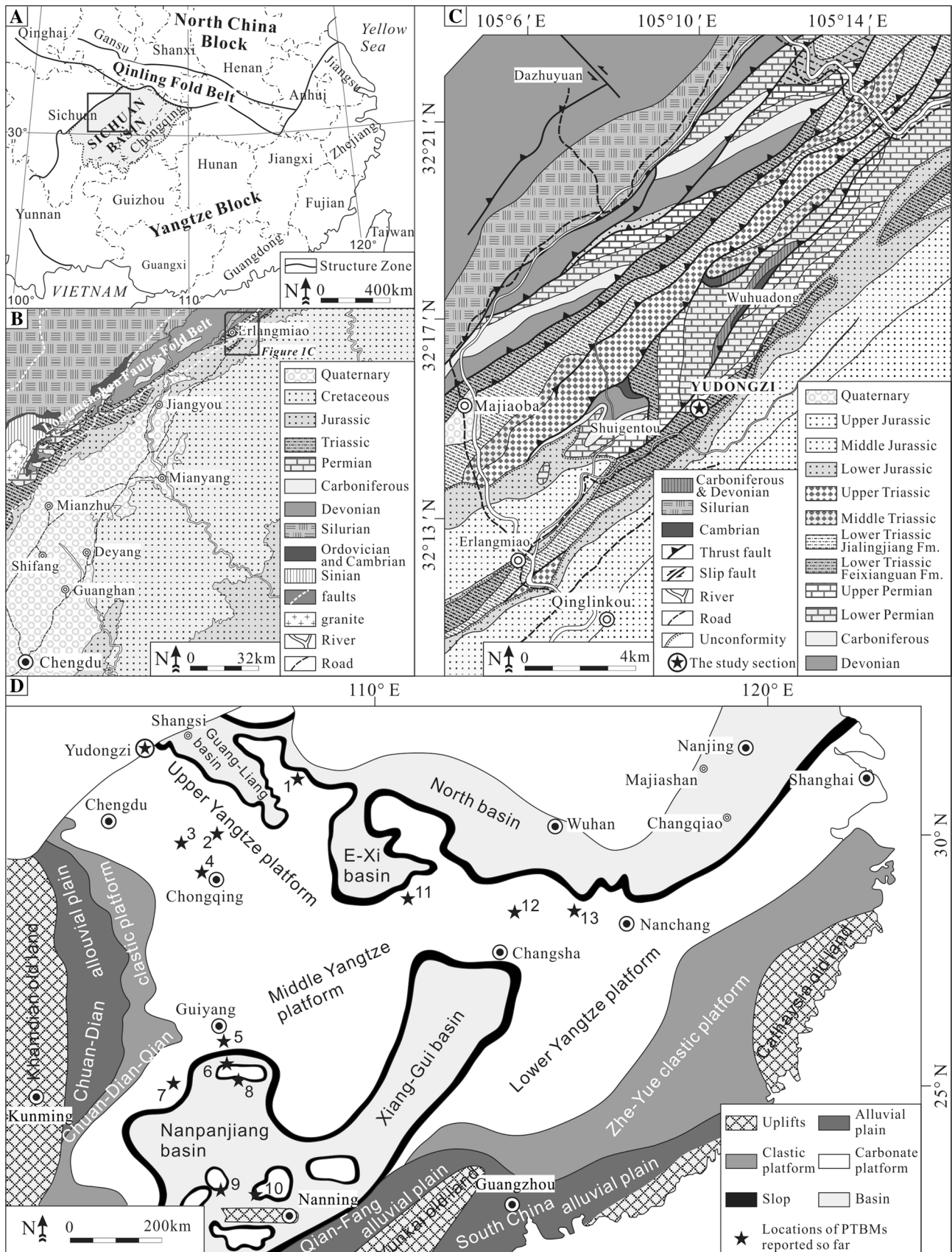


**Fig. 1** Geologic settings and the study section location. **a** Structural map of South China and location of Sichuan Basin (grey) (modified from Lehrmann et al. 2003). **b** Geological map of the northern Sichuan Basin (rectangle block in **a**) (Yao et al. 2002). **c** Summary of geology and location (asterisk) of section of the study area (rectangle block in **b**) (Yao et al. 2002). **d** Paleogeographical maps of South China during Permian–Triassic transition, after Liu et al. (2014). Stars represent locations of PTBM reported so far in South China, they are 1 Panlongdong, 2 Huayingshan, 3 Tudiya, 4 Laolongdong, 5 Luodian, 6 Dajiang, 7 Ziyun, 8 Heping, 9 Zuodeng, 10 Taiping, 11 Cili, 12 Chongyang, 13 Xiushui

et al. 2008; Kershaw et al. 2007, 2009, 2011; Yang et al. 2011; Forel et al. 2013; Kershaw et al. 2012; Loope et al. 2013; Jiang et al. 2014; Wu et al. 2014; Lehrmann et al. 2015; Wu et al. 2016). Microbialites also occur later in the Early Triassic (Schubert and Bottjer 1992; Lehrmann 1999; Pruss and Bottjer 2004; Pruss et al. 2006; Mary and Woods 2008; Mata and Bottjer 2011; Marengo et al. 2012; Chen et al. 2014; Vennin et al. 2015), where they are commonly described as having formed in anoxic, harsh environments (e.g., Pruss and Bottjer 2004; Pruss et al. 2006; Mary and Woods 2008; Mata and Bottjer 2011).

PTBMs reported so far are mostly stromatolites and thrombolites (Kershaw et al. 2012 and references therein). They are abundant in low-latitude Tethyan locations including South China, Vietnam, Saudi Arabia, Turkey, Iran, and Hungary, and formed mostly in shallow subtidal environments but also occurred in the deeper shelf, seamounts, and rift basins (Kershaw et al. 2012 and references therein). The models for their generation consist of a series of viewpoints, including: (1) reduced benthic grazing pressure; (2) upwelling of anoxic alkaline waters; (3) elimination of skeletal  $\text{CaCO}_3$  sinks; (4) increased nutrient levels from erupted volcanic ash; and (5) a rebound in carbonate saturation following a transient ocean acidification event (Lehrmann et al. 2015 and references therein). The upwelling model, in particular, has been applied by numerous workers in the Early Triassic (Kershaw et al. 1999; Ezaki et al. 2003; Lehrmann et al. 2003; Pruss and Bottjer 2004; Pruss et al. 2005; Kershaw et al. 2007, 2009, 2011; Ezaki et al. 2008; Mary and Woods 2008; Mata and Bottjer 2011; He et al. 2013; Woods 2014). Lehrmann et al. (2003) also drew attention to the possibility of PTBM formation in oxygenated seawater conditions. The paleoceanographic environments (such as anoxia and high temperature) were thought to be the main contributing factor to the delayed Early Triassic biotic recovery (Song et al. 2014). As a diagnostic unusual sedimentary record, PTBMs are thus generally regarded as indicators of anoxic, severe environments (e.g., Pruss et al. 2006; Knoll et al. 2007; Mary and Woods 2008).

However, some recent studies show that the formation of PTBMs might occur in oxygenated environments,

suggested by Lehrmann et al. (2015). Liu et al. (2010) discovered that filter-feeding ostracods accounted for only 9% of ostracods of PTBMs in Chongyang (South China), suggesting a marine environment with normal oxygen level; filter feeders have a greater tolerance to low oxygen than deposit feeders, so a low ratio of filter feeders to deposit feeders suggests higher oxygen levels. Forel et al. (2013) also reported ostracods assemblages, indicating oxygenated conditions within PTBMs in Dajiang (South China), Bálvány North (Hungary), and Çürük Dağ (Turkey). In addition, Loope et al. (2013), based on geochemical analyses of rare earth elements and iodine of the PTBMs from Demirtas (Turkey) and Cili (South China), concluded that they both developed in an oxygen-rich environment. Moreover, Collin et al. (2014) interpreted oxic conditions prevailed during the growth of PTBMs according to the analysis of U, V, Mo, and REE (Ce anomaly). The above studies not only present the complexity of redox conditions during the Permian–Triassic transition but also pose a challenge to the prior interpretation that PTBMs can indicate Early Triassic distressed marine environments associated with anoxia. As the characteristic feature of the Early Triassic shallow-marine environments, PTBMs are of significance in understanding changing paleoenvironments associated with the End-Permian extinction, as well as help to explain the delay of biological recovery in the Early Triassic. Thus, it is necessary to reassess the paleoenvironment of the PTBMs, especially in terms of redox conditions.

In addition, in eastern Tethys, most PTBMs reported so far occur abundantly in several areas of the Yangtze platform (i.e., South China and Vietnam) including the northern margins of Middle and Lower Yangtze platforms (i.e., in central and eastern China), and isolated platforms within Nanpanjiang basin. The distributions and thickness of PTBMs on Upper Yangtze platform are few and limited. The examples from Laolongdong, Dongwan, and Baizhuyuan (Sichuan) revealed the thickness of PTBMs are ca. 2 m on average and maximum of ca. 3 m (Kershaw et al. 2012). Similar to most other shallow-water sections in South China, the thickness of PTBMs are definitely thinner than those from western Tethys, such as Çürük Dağ in southern Turkey (ca. 15 m), Bükk Mountains in Hungary (ca. 5 m) and Aliquordaz in Iran (ca. 5 m) (Kershaw et al. 2012). Our new work revealed PTBMs developed on the north margin of Upper Yangtze platform with remarkable thickness (up to 11 m), which is much thicker than most other shallow-water sections in the eastern Tethys. It may offer a higher-resolution and more complete record to further understand the initial recovery process in the eastern Tethys during this period. We thus chose an ideal representative section, 11 m thick, well exposed in the Yudongzi section, Sichuan, China (Fig. 1), for detailed analysis, and assessed the stratigraphic variation in abundance and size of metazoan fossils

within microbialites, as well as analyzed the TOC and TS abundance through the microbialite beds. The results of our investigations lead us to question the applicability of PTBMs as indicators of anoxic, harsh environments in the aftermath of latest Permian extinction.

### Geologic setting

The Sichuan Basin (Fig. 1a) in the northwest part of Upper Yangtze platform has a complicated history; it was a passive margin during Neoproterozoic to Middle Mesozoic time but changed into a foreland basin during Late Mesozoic to Cenozoic (Wang 1989). In the northeast of the basin, the north margin of Upper Yangtze platform, Permian and Triassic strata are widely exposed in front of the Longmenshan fault-fold belt (Fig. 1b) and Permian–Triassic boundary sections are well developed. The studied section is located in the Yudongzi area (Fig. 1c) near Erlangmiao Town, in the district of Jiangyou City, northwestern Sichuan Basin.

The Upper Permian near Erlangmiao Town is represented, from older to younger, by the Wujiaping Formation, consisting of grey medium- to thick-bedded skeletal

grainstone with banded chert, and medium- to thin-bedded lime mudstone, and Changxing Formation consisting of grey thick-bedded sponge and coral boundstone and medium- to thick-bedded skeletal grainstone with nodular chert (Fig. 2a) (Wang 1989; Tan et al. 2012; He et al. 2015). The beds of both Wujiaping Formation and Changxing Formation contain a rich biota of algae, foraminifers, sponges, anthozoans, bivalves, gastropods, nautiloids, ostracods, trilobites, brachiopods, bryozoans, echinoderms, scolecodonts, conodonts, and chondrichthyes (Rong et al. 2009; Wang et al. 2009; Tan et al. 2012; He et al. 2015). The Wujiaping Formation is in comfortable contact with the overlying Changxing Formation, but in unconformable contact with the underlying Middle Permian Maokou Formation, which consists mainly of grey to black thick-bedded skeletal packstone with nodular and banded chert (Fig. 2a). The Wujiaping Formation here has been interpreted to represent marginal shoals of the carbonate ramp, which developed in the Sichuan basin at the beginning of Late Permian time (He et al. 2015), while the Changxing Formation has been interpreted to represent marginal reefs of the rimmed carbonate shelf, which originate from the Wujiaping Formation ramp steepening distally during the

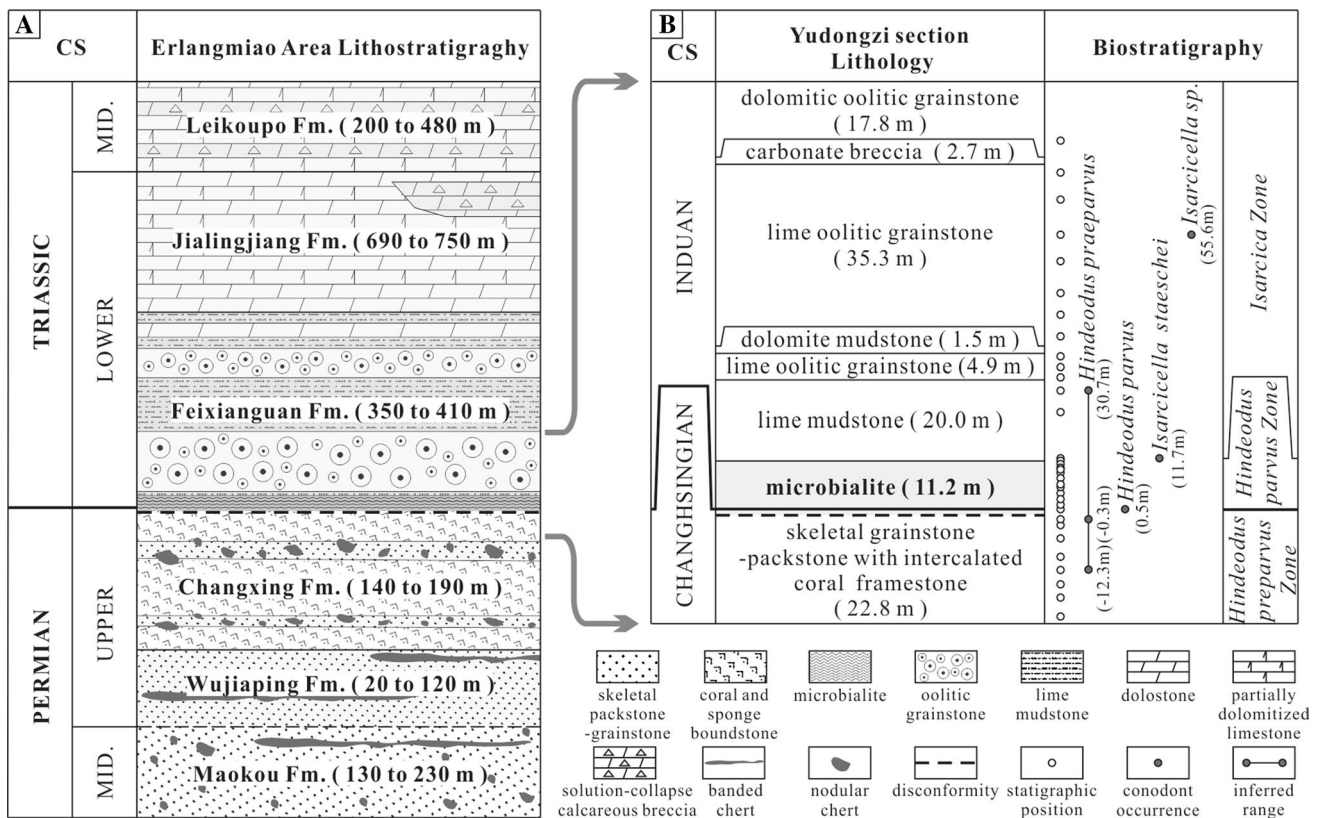


**Fig. 2** Stratigraphic setting of the Upper Permian and Lower Triassic Formations in the study area. **a** General scheme of the Permian and Lower–Middle Triassic lithostratigraphy in the study area, after

Rong et al. (2012). **b** Lithological units (after Rong et al. 2012) and biostratigraphical subdivision of the uppermost Permian–lowermost Triassic. CS chronostratigraphy, *Fm* formation



later part of Late Permian transgression (Tan et al. 2012). It should be noted that the Changxing Formation occurs only in the carbonate platform area but was equivalent to the Dalong Formation developed in slope and basin environments (Fig. 1d), which consists mainly of alternations of black thin-bedded calcareous mudstones, laminated marls and grey to black thin-bedded limestone. Also, the contact between the Dalong Formation and the overlying Feixianguan Formation is comfortable.

The Lower Triassic in the Erlangmiao area is represented, from older to younger, by Feixianguan Formation and Jialingjiang Formation, which are in conformable contact with each other (Fig. 2a) (Wang 1989). The Feixianguan Formation consists of, from older to younger, grey massive microbialites with thick-bedded oolitic grainstone, interbedding of red-colored thin-bedded silty mudstone and marlstone, red thin-bedded silty mudstone-marlstone with grey-white medium-bedded oolitic grainstone, and red shale-marlstone occasionally with khaki-colored thin-bedded dolomitic mudstone (Fig. 2a) (Wang 1989; Rong et al. 2012). The Jialingjiang Formation consists of light grey or yellow grey thin- to thick-bedded partially dolomitized limestone and dolostone, and bedded solution-collapse calcareous breccia (Tang et al. 2014) in some parts. The Jialingjiang Formation is overlain conformably by the Leikoupo Formation, which is mainly made up of cyclic alternations of bedded partially dolomitized limestone, dolostone, and solution-collapse calcareous breccia (Fig. 2a) (Wang 1989). The Feixianguan Formation at Yudongzi section has been interpreted to represent marginal shoals of the rimmed carbonate shelf, which evolved from the Changxing Formation rimmed shelf but mainly consists of oolitic grainstone rather than skeletal grainstone in the shelf margin area (Rong et al. 2012). However, the environment represented by the Jialingjiang Formation there is interpreted as a carbonate tidal flat due to the regression and restriction by surrounding ancient lands and submarine uplifts during the Middle Triassic in the Sichuan Basin (Tang et al. 2014).

At Yudongzi, the Feixianguan Formation consists of, from older to younger, mainly microbialites, lime mudstone, lime oolitic grainstone, dolomite mudstone, lime oolitic grainstone, carbonate breccia, and dolomitic oolitic grainstone (Fig. 2b). The Changxing Formation consists of thin-bedded skeletal packstone with coral-rich lenses (Fig. 2b). Two uneven erosion interfaces exist in the top beds of the Changxing Formation, one close to the top and the other defines the top of the Changxing Formation. Weathered skeletal packstone filled in low-lying parts of the lower erosion surface (Fig. 3c) and comprised of intraclasts supported by mud matrix, with sand-sized and gravel-sized grains of different sizes, poorly sorted and ranging from subangular to subrounded (Fig. 3d, e). This surface is interpreted here as an in situ epigenetic karst

structure (Fig. 3c–e), thus the contact between Changxing Formation and Feixianguan Formation is inferred to be a disconformity (Figs. 2, 3b).

## Methods

### Sampling and preparation

Thirty-three large samples with an individual sample weight of more than 10 kg were collected from Yudongzi section (Fig. 2b). Twelve of the total 33 were collected from the microbialite (numbered Y1–Y12 in Fig. 4), and these were divided into two portions: (1) one for detailed petrographic study and measurement of TOC and TS; and (2) the other for conodont identification along with the rest of the 33 samples. Samples for conodont study were fragmented to pieces of ca. 1-cm diameter. The 12 microbialite samples were firstly made into polished slabs with a size of 15 × 10 × 5 cm and then subdivided into 30 pieces for 10 × 6 cm thin-sections. Some of the polished slabs were immersed in ca. 5% acetic acid for 4–5 days to be made into acid etched slabs. The slabs and thin-sections are prepared for petrology and statistical analysis.

### Age constraints

The age of the Yudongzi PTBMs sequence was determined on the basis of conodonts. Through the preparation, 33 conodont samples (each one weighing ca. 10 kg on average) were collected, and then were processed following the procedure implemented by Jiang et al. (2007).

### Microbialite description

The Yudongzi PTBMs were described in four size scales (Shapiro 2000; Ezaki et al. 2003, 2008) defined as: (1) megastructure that characterizes the stratum of PTBMs in general; (2) macrostructure that characterizes the appearance of the construction of all the kinds of microbialites in the megastructure; (3) mesostructure that describes the details in the macro structure that are visible in hand specimen; and (4) microstructure which gives information on the composition and features of the mesostructure under the microscope. The first three were implemented by characterizing outcrops in the field, and observing polished slabs and acid-etched slabs in the laboratory, while the microstructure was characterized by thin-section study.

### Taxon, abundance, and size statistics of metazoan fossils

Thin-sections were observed and photographed with a Nikon ECLIPSE LV100N POL microscope with 10×

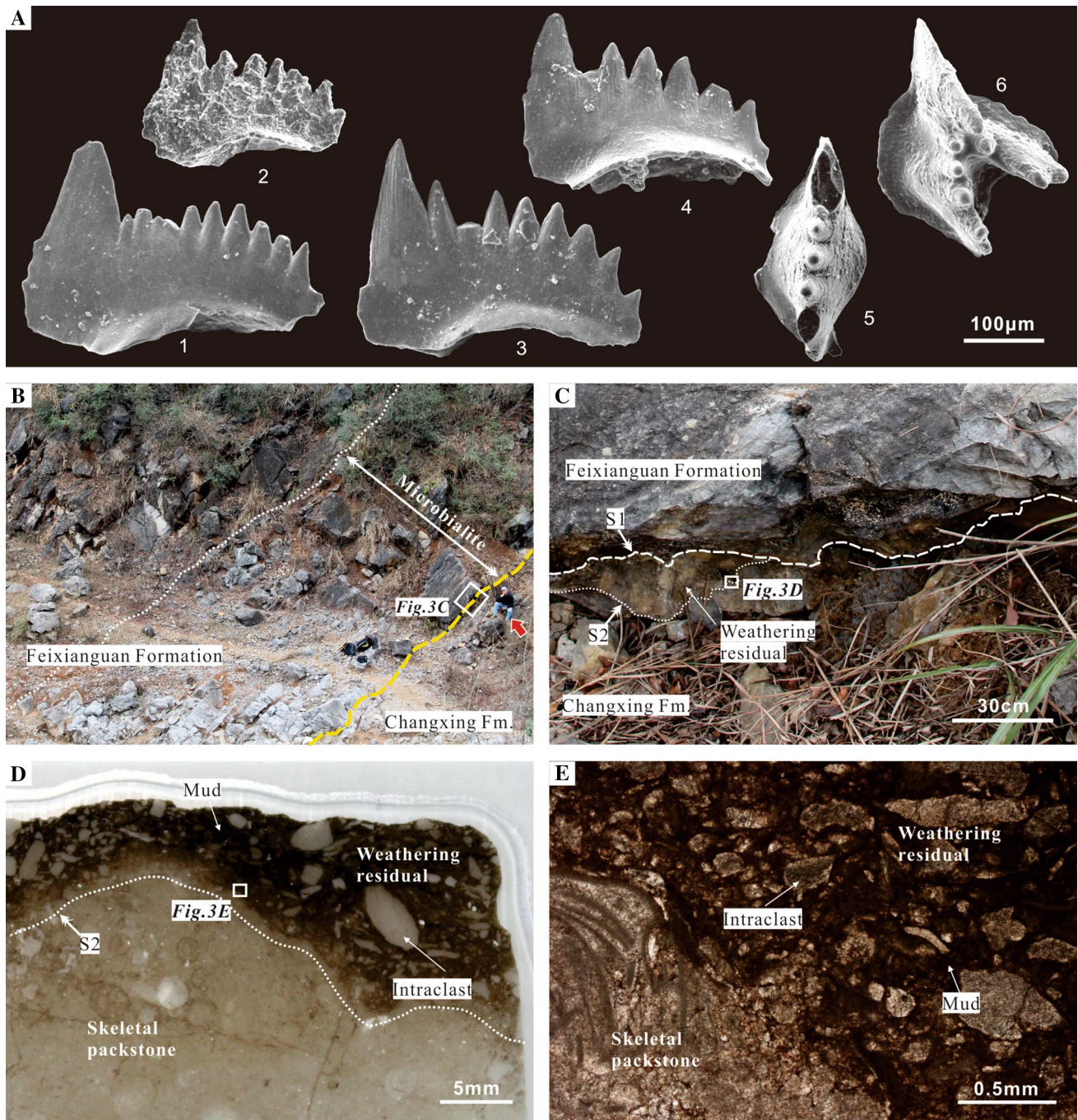


**Fig. 3** Photographs of conodont fossils from the studied section, and disconformity surface on the top of Changxing Formation. **a** 1 *Hindeodus parvus*, 2–4 *H. praeparvus*, 5 *Sarcicella staeschei*, 6 *I.sp.* **b** Outcrop view of PTB section at Yudongzi (see Fig. 2). Microbialite beds (megastructure) are laterally contiguous and vary in thickness. Yellow dotted line demarcates the top of Changxing Formation. The contact between Changxing Formation and Feixianguan Formation is a disconformity. White line demarcates the topside of the microbialite. Person for scale (red arrow); **b** detail of area in **b** (rectangle on **b**). Two irregular erosions (S1 and S2) developed at the top of

Changxing Formation, and the potholes of S2 are often filled with the weathering residual. **d** Photograph of thin section of the weathering residual (sampled from the rectangle on **c**), which consists of poorly sorted, subangular to subrounded intraclasts supported by mud. The boundary between weathering residue and skeletal packstone (the parent rock) is ambiguous and there is a transition zone between them. **e** Close-up view of the rectangle on **d**. The intraclasts and other debris formed from the dissociation of the skeletal packstone, suggesting that they were accumulated in situ



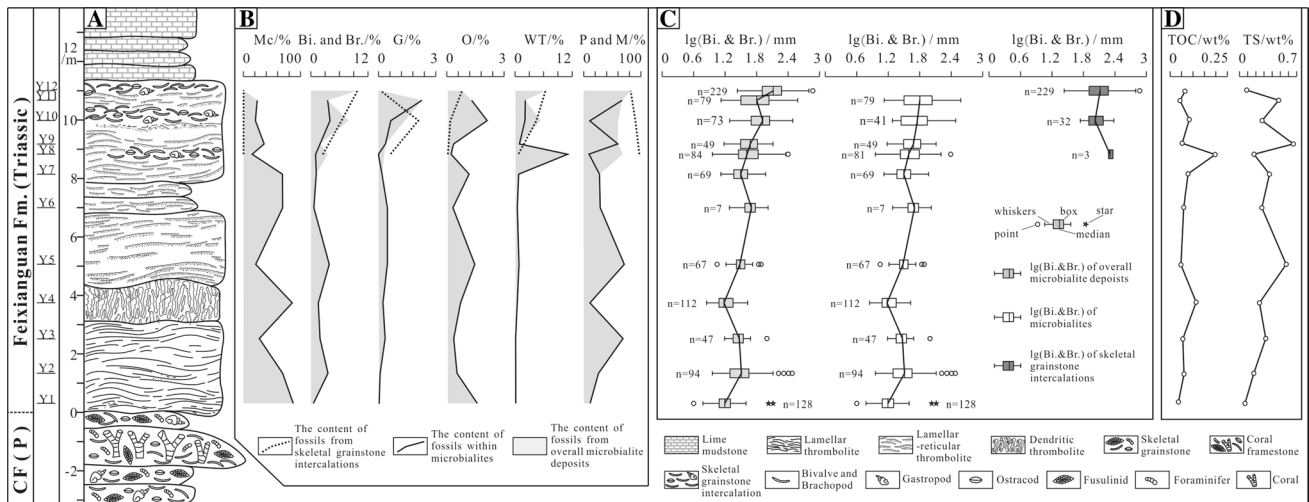


**Fig. 4** Comprehensive column of the Yudongzi PTBM succession. Y1 to Y12 are sample numbers, and these 12 samples were collected through the microbialite to assemble a representative suite of samples of the microbialite. **a** Lithologic column of the Yudongzi PTBMs. **b** Changes in the abundance of metazoan fossils and other fabrics of microbialites through the succession. **c** Box plots of the lg (Bi. & Br.) showing the changes and distribution of sizes of bivalve and brachiopod fossils through the microbialite beds. Boxes encompass 25th through 75th percentiles, with the median marked by a central

line. The whiskers are drawn from the top of the box up to the largest data point less than 1.5 times the box height from the box (the “upper inner fence”), and similarly below the box. Values outside the inner fences are shown as circles, values further than three times the box height from the box (the “outer fences”) are shown as stars. *N* represents the number of bivalve and brachiopod shells in each sample. **d** Abundances of TOC and TS of microbialites through the succession. *Mc* mesoclots, *Bi* bivalve, *Br* brachiopod, *G* gastropod, *O* ostracod, *WT* worm tube, *P* peloid, *M* (peloidal) micrite

eyepiece lens and 1.25× objective lens. Then the percentage of each taxon in the photographs of sections was calculated by point counting; the detailed procedure of point counting followed the method described by Payne et al. (2006). Finally, these data were processed using EXCEL where a bar chart of the proportion of each taxon was developed. For the metazoan fossils size statistics, the maximum linear dimension (MLD) of each specimen in the photographs was documented so that the box chart of MLD of each taxon in the microbialite succession could be developed by the PAST software (Hammer et al. 2001). MLD is highly correlated with biovolume, capturing approximately 90% of variance in biovolume in a study of diverse fossil groups (Novack-Gottshall 2008), and therefore can serve for the size statistics of metazoan fossils.

**TOC and TS analyses**

The samples were powdered and sieved through a 200-mesh screen, then treated for 12 h with hot 2 N HCl to remove all carbonates and other acid-soluble minerals. Approximately 100 mg of powdered sample was combusted and analyzed on a CS230 carbon and sulfur analyzer for total organic carbon and total sulfur at State Key Laboratory of Oil and Gas Reservoir Geology and Exploitation, Chengdu, China. USGS SDO-1 standard sample was used as the control sample in the experiment, and the deviation in the carbon and sulfur test results is less than 2.5 and 5%, respectively.

**Results**

**Age**

Three conodont biozones were distinguished in the studied section (Fig. 2b), in ascending order they are *Hindeodus praeparvus* Zone, *H. parvus* Zone and *Isarcicella* Zone. The *Hindeodus praeparvus* Zone occurs at the top of Changxing Formation, ending with the first appearance datum (FAD) of *H. parvus* at 0.5 m above the base of Feixianguan Formation. The overlying conodont biozone, the *Hindeodus parvus* Zone, occurring 0.5 m above the base of Feixianguan Formation, starts at FAD of *H. parvus* and ends with the FAD of *Isarcicella staeschei* (11.7 m above the base of Feixianguan Formation). The uppermost zone found in these samples is *Isarcicella* Zone starting at FAD of *Isarcicella staeschei*. The FAD of *H. parvus* may be moved down if more *H. parvus* fossils are identified at the lower position in future work. The Yudongzi PTBMs thus mainly occur in the *Hindeodus parvus* Zone but may cross the Permian–Triassic boundary.

**Microbialite mega- to microstructures**

The Yudongzi PTBMs are all thrombolite form. The megastructure displays a set of horizontally continuous-bedded thrombolites with relevantly uniform thickness (Fig. 3b),

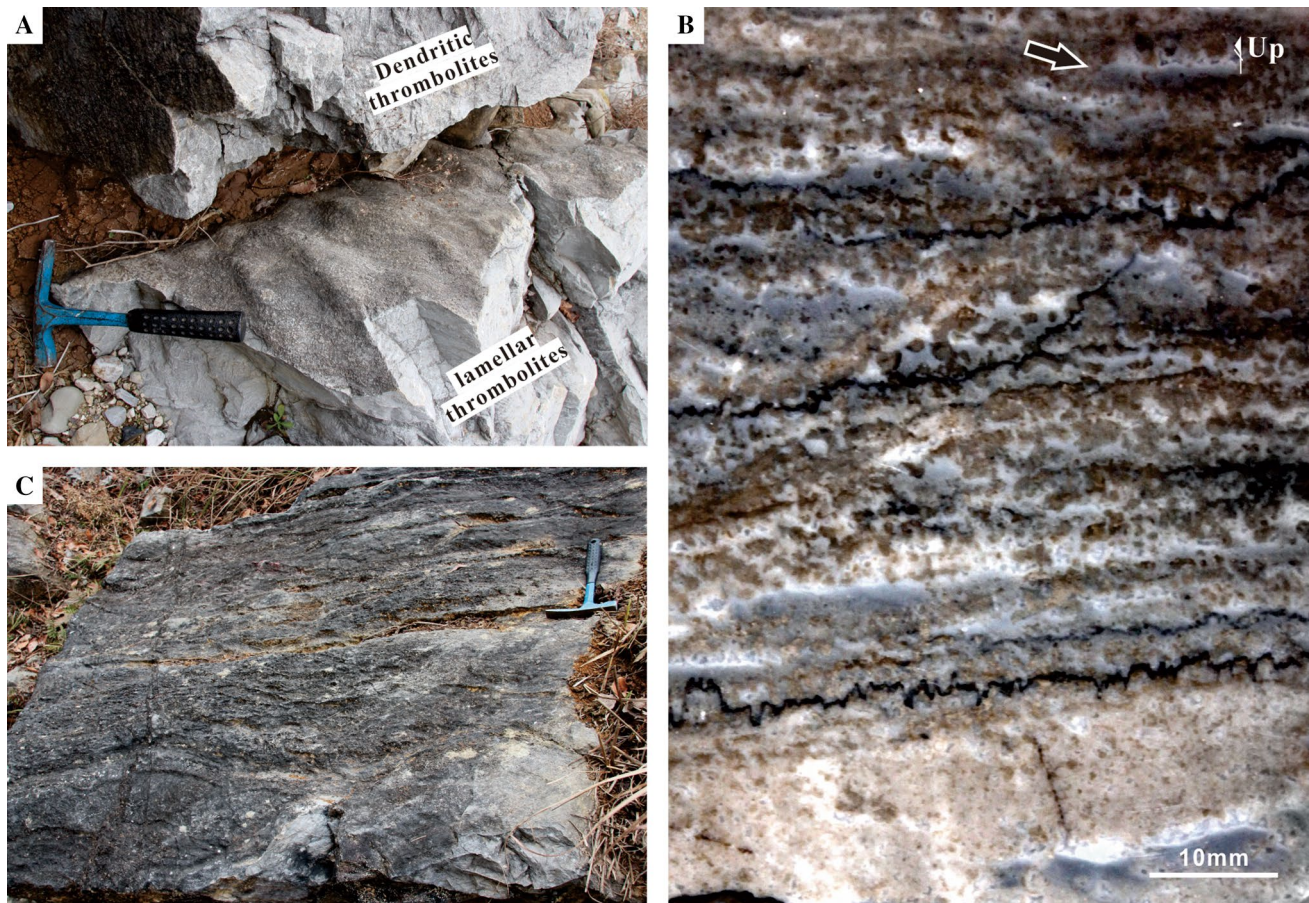


**Fig. 5** Photographs of macro- and mesostructures of the lamellar thrombolite. **a** The top of undulating lamellar thrombolites shows many directed small bulges of which the *long axes* are mostly in the same direction. **b** Undulating lamellar mesostructure. *Geological hammer* 30 cm long. **c** Polished slab of lamellar mesostructure. *Chocolate-colored spots* are mesoclots, which amalgamate with each other to form frameworks of the lamellar thrombolite. Spaces (such

as the *black arrow*) between mesoclots are filled with peloids, micrite, and spar. Peloids and micrite are the *grey* lower fillings of the spaces, whereas spar is *white* and filled in the *upper parts*, exhibiting a geopetal texture. Peloids and micrite can not be differentiated from each other on the slab but can be observed very well under the optical microscope (see Fig. 6). Abbreviations as in Fig. 4

while the macro-, meso-, and micro-structures vary significantly from layer to layer. For the mesostructures, we classified the Yudongzi PTBMs into three types, lamellar thrombolites, dendritic thrombolites, and lamellar-reticular thrombolites.

Lamellar thrombolite, 3.1 m in thickness, is seen at the lowermost part of the Yudongzi PTBMs (Fig. 4). At the macroscopic scale, lamellar thrombolite is bedded (Fig. 5c) and has an undulating surface where lots of small bulges developed. These bulges are strip-shaped, measured as 20–30 cm long, 5–10 cm wide, and 1–5 cm thick, and thin from the center to the periphery (Fig. 5a). On the mesoscopic scale, the lamellar thrombolites are characterized by the development of undulating lamellar mesostructures (Fig. 5b), which are composed of spotted mesoclots (Shapiro 2000) with a diameter of 1–2 mm connecting and merging with each other (Fig. 5c). On the microscopic scale, the

mesoclot features ambiguous boundaries, and is composed of micrite, (micro-) spar from recrystallization (Fig. 6a, c) and dolomite (Fig. 6e, f). In some cases, a small number of hollow coccoidal microbes are free of influence of diagenesis, being reserved within outer parts of mesoclots (Fig. 6f). Mesoclots built the microbialite framework containing cavities normally full of spars, peloids, micrite, bioclasts, and few pyrite (Fig. 6). Relatively large cavities are geopetally filled in many cases (Fig. 6a–d).

Dendritic thrombolite, 1.3 m thick, developed on the top surface of lamellar thrombolite (Fig. 4). On the macroscopic scale, the dendritic thrombolite is of domal growth habit, shown by dome developing on its top (Fig. 7a, b). On the mesoscopic scale, the interior of dendritic thrombolite shows dendritic mesostructure, which is vertically orientated and perpendicular to the bottom surface of the microbialite (Fig. 7a). The dendritic mesostructure is



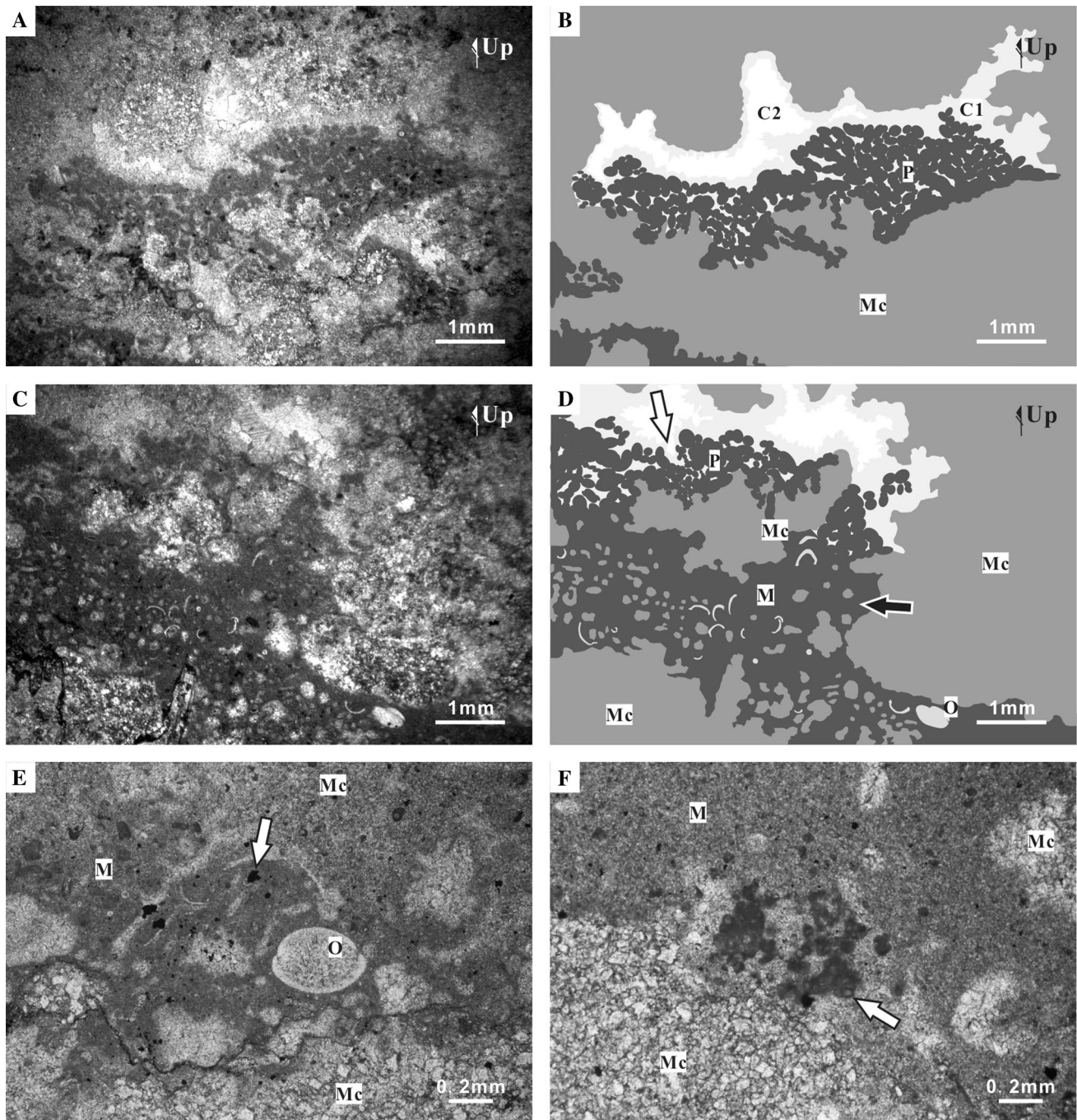


**Fig. 6** Photographs of microstructure of the lamellar thrombolite. **a**, **b** is the line drawing of **a**. Mesoclots feature irregular boundaries, and are composed of a considerable amount of mosaic spar due to recrystallization. The space between mesoclots is mostly filled with two-phase spar cements in the upper part and a large number of peloids in the lower part, exhibiting a geopetal texture. **c**, **d** is the line drawing of **c**. When the space between mesoclots is relatively large, the peloids in the lower part of the space are indistinct in outline (*black*

*arrow*), owing to compaction into peloidal micrite, whereas their outlines are distinct in the upper part of the sediment filling (*white arrow*). **e** Few pyrite (*white arrow*) scattered in fillings between mesoclots which is recrystallized and contains dolomite crystal. **f** Hollow coccoidal microbes (*white arrow*) free of diagenesis destruction in some cases, are reserved in the outer part of mesoclots. **C1** 1st phase cement is fibrous to bladed spar, **C2** 2nd phase cement is mosaic spar; all others as in Fig. 4

composed mainly of dendritic mesoclots 0.5–1 cm wide and 7–8 cm long being superposed on one another (Fig. 7c, d). On the microscopic scale, dendritic mesoclots consist

of ellipsoid-shaped small clots with a long diameter ranging from 3 to 4 mm. Part of the small clots have coccoidal microbes of 0.1–0.3 mm diameter mounted in them



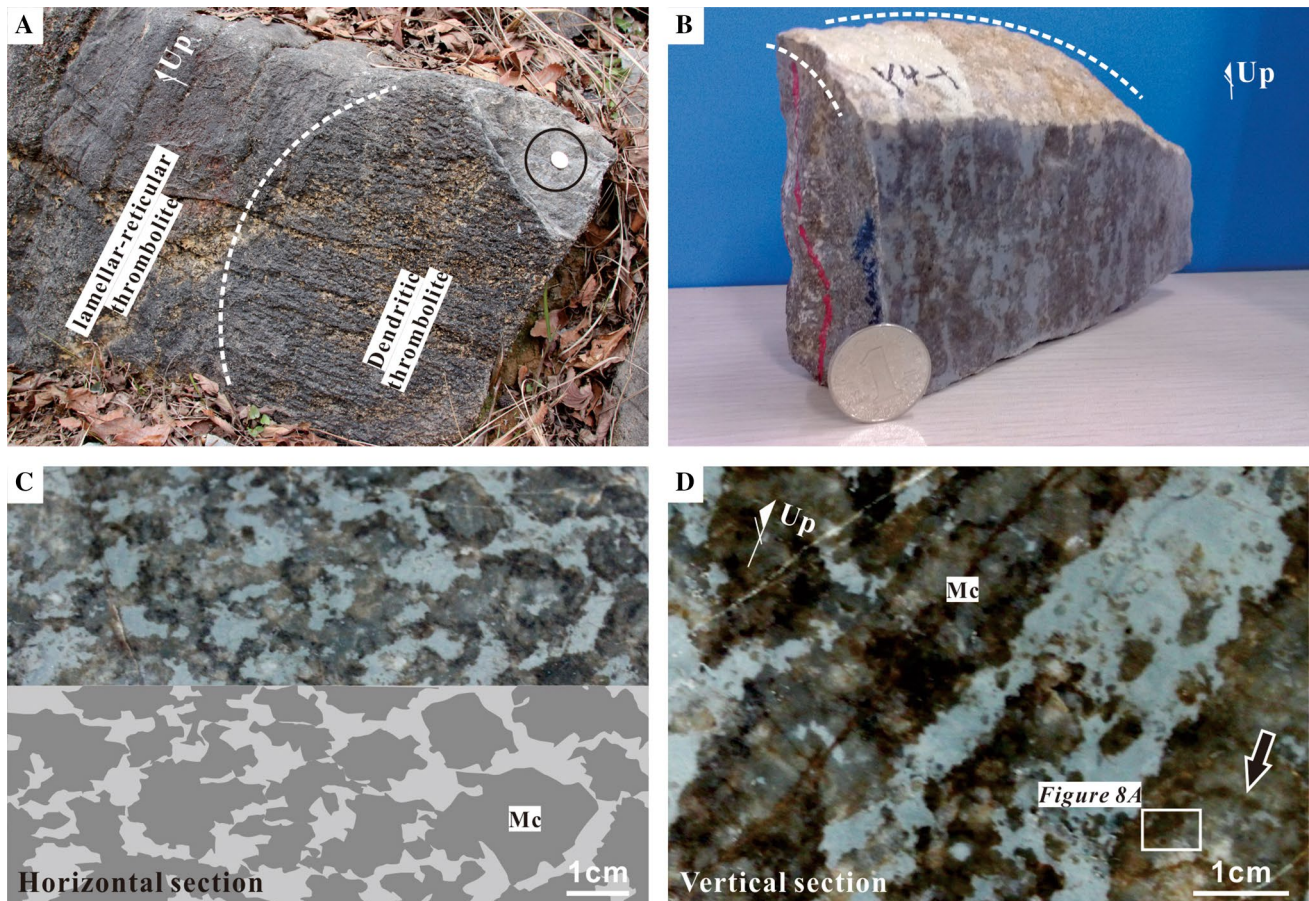


**Fig. 7** Photographs of macro- and mesostructures of the dendritic thrombolite. **a** Mound-like structures with a dome in dendritic thrombolite, no erosion surface between the dendritic thrombolite and its overlying lamellar-reticular thrombolite. Dendritic mesostructures inside are perpendicular to the surface. Diameter of the *coin* is 1.5 cm. **b** A hand specimen from the top of dendritic thrombolite. Notice its arched top. Diameter of the *coin* is 2.5 cm. **c** Horizontal

section of individual dendritic mesoclot is an irregular ellipse, and part of the dendritic mesoclots are horizontally connected. The lower part of **c** is a line drawing of the upper part. **d** Vertically, the dendritic mesoclot alternates with another, and arched laminae (*black arrow*) made up of small clots that can be seen inside them under optical microscope (see Fig. 8a, b). Abbreviations as in Fig. 4

(Fig. 8a, b). Spaces between small clots are mostly filled with two phases of spar cements (Fig. 8a), while between dendritic mesoclots fill peloids, peloidal micrite, bioclasts, and rare pyrite (Fig. 8c, d).

The uppermost part of the Yudongzi PTBM is lamellar-reticular thrombolite (Fig. 4), 6.8 m in thickness, with a smooth transition to the underlying dendritic thrombolites, and no obvious exposed erosion surface is seen between the two (Fig. 9a). At the macroscopic scale, the lamellar-reticular thrombolites, similar to the lamellar thrombolites, are identified as an undulating bedded microbialite and interlaid with several layers of skeletal grainstone (Figs. 4, 9c). On the mesoscopic scale, compared to the lamellar thrombolite, the laminae of lamellar-reticular thrombolite are more divergent, and mostly vertically connected (Fig. 9a). The interior of the structure is mainly characterized by coarsely clotted and striped mesoclots, which

are mainly horizontally connected and partially vertically connected, giving the microbialite a gridded appearance (Fig. 9b). At the microscopic scale, except for partial recrystallization, the interior of the mesoclots is mainly characterized by ellipsoid or irregularly capsular small clots (Fig. 10a), ca. 0.1 mm diameter, which are often fringed with several ca. 0.01-mm—diameter micro-spherical structures (Fig. 10b) resembling coccoidal microbes. Spaces between mesoclots are filled with biodetritus and micrite (Fig. 10c), while the space between biodetritus of the skeletal grainstone is mainly filled with peloids (Fig. 10d).

#### Trends in abundance and size of metazoan fossils

Metazoan fossils of the Yudongzi PTBM succession occur within microbialites and skeletal grainstone intercalations



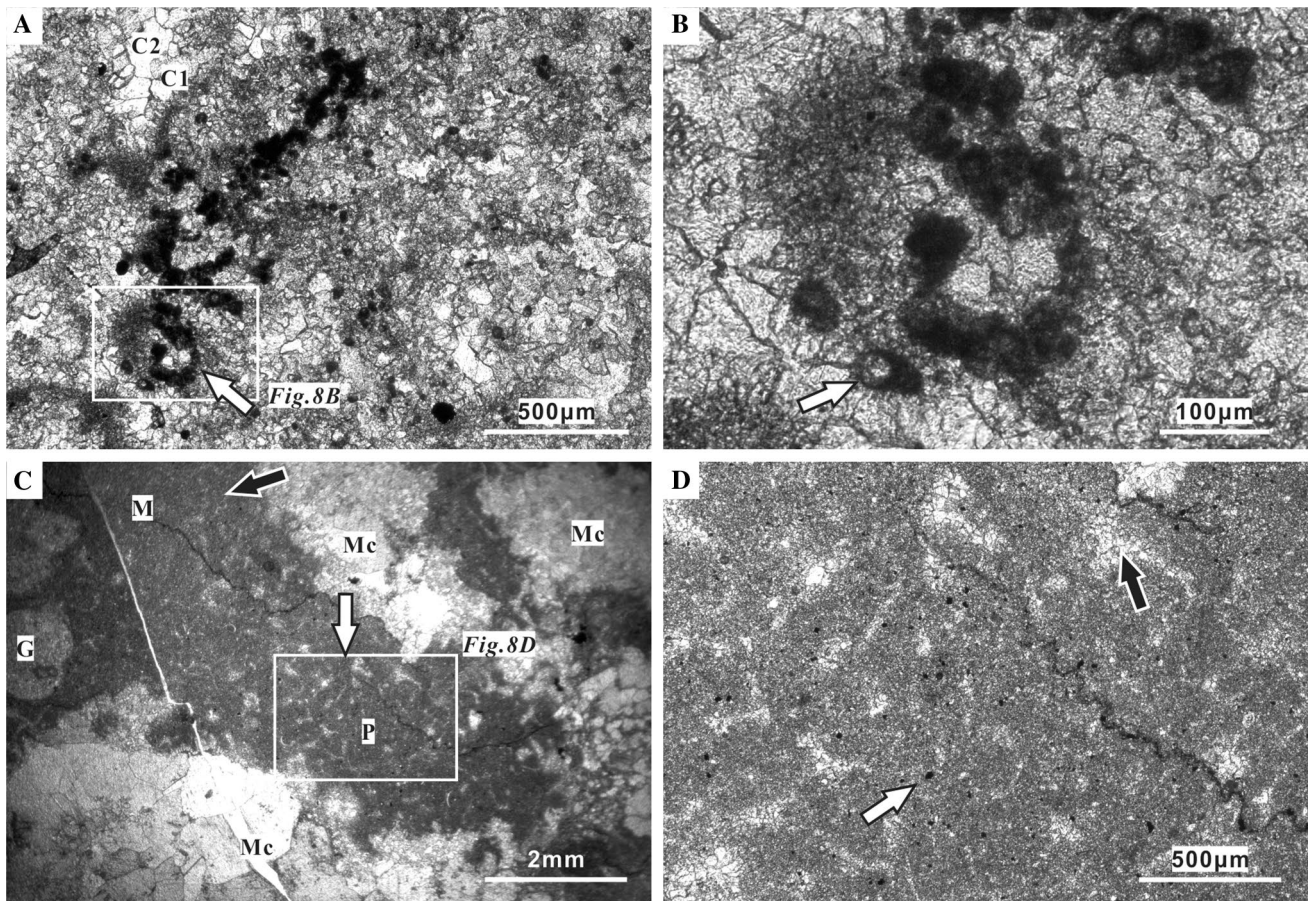


**Fig. 8** Photographs of microstructures of the dendritic thrombolite. **a** Close-up of the *rectangle* on Fig. 7d. The laminae (see Fig. 7d) in dendritic mesoclot on the slab are identified under the microscope as an arched arrangement of small clots. Spaces between small clots are filled with two-phase spar cements. **b** Details of small clots (*rectangle* on **a**). Inside the small clots is sparry calcite, and some hollow coccoidal microbe (*white arrow*) occur in the edges. **c** Between the dendritic mesoclots are areas of micritic sediment, comprising

clear peloids (*white arrow*), grading to areas of micrite with a vague peloidal texture and may be composed of compressed peloids (*black arrow*) and biotritus. **d** Close-up view of tangle area in **c**: space between micrite peloids is filled with spar cements (*black arrow*). A few pyrites (*white arrow*) also scattered there. C1 1st phase cement is fibrous to bladed spar, C2 2nd phase cement is mosaic spar; all others as in Fig. 4

(Fig. 4), including bivalves, brachiopods, worm tubes, gastropods, and ostracods (Table 1). For the overall microbialite deposit (microbialites and skeletal grainstone intercalations), brachiopods and bivalves (here we regarded brachiopods and bivalves as one category due to the difficulty of differentiating them when they are small) account for the highest portion, worm tubes (2.3% on average) take second place, and ostracods (0.9% on average) and gastropods (0.5% on average) take up the least portion (Table 1). The content of metazoan fossils within the microbialites demonstrate a similar character (brachiopods and bivalves, 2.2% on average; worm tubes, 1.7% on average; ostracods, 0.9% on average; gastropods, 0.3% on average), so does the abundance of metazoan fossils in the skeletal grainstone intercalations (brachiopods and bivalves, 6.3% on average; worm tubes, 3.8% on average;

gastropods, 0.8% on average; ostracods, 0.3% on average) (Table 1).

We assessed the stratigraphic variation of abundance of metazoan fossils (Fig. 11a–j), and found: (1) for the overall microbialite deposit, the content of total metazoan fossils and the stratigraphic position exhibit a good positive correlation, with the equation of linear regression being  $y = 1.02x + 0.37$ , correlation coefficient being 0.63 (Fig. 11a). Even each taxon demonstrates a positive correlation with the stratigraphic position (Fig. 11b–e). For instance, bivalves and brachiopods (coefficient of 0.53), and worm tubes (coefficient of 0.59) have a high positive correlation with the stratigraphic position (Fig. 11b, c). Gastropods (coefficient of 0.31) and ostracods (coefficient of 0.10), however, demonstrate a relatively weak positive correlation with the stratigraphic position and a slow



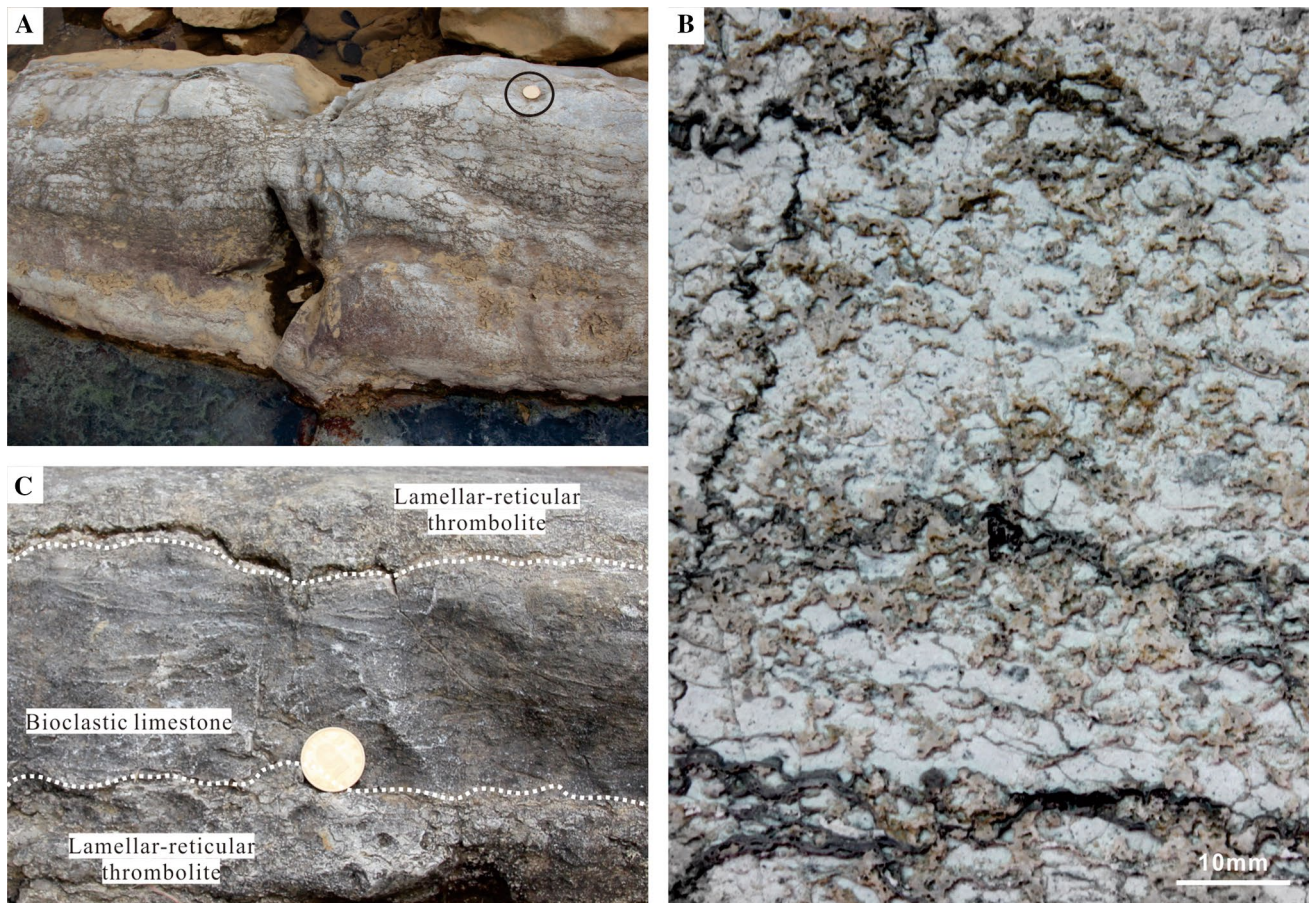


**Fig. 9** Photographs of macro- and mesostructures of the lamellar-reticular thrombolite. **a** Outcrop of lamellar-reticular mesostructures, with diffuse laminae and vertical crosses. Diameter of *coin* is 1.5 cm. **b** Acid-etched slab of lamellar-reticular mesostructure. The brown porphyritic to striped mesoclots are mainly horizontally connected and partially vertically connected, with a feature of gridding.

Between the mesoclots is a fill of off-white micritic limestone with biotritus. **c** Thin interlayers of skeletal grainstone with ambiguous cross-bedding are identified inside lamellar-reticular thrombolites. *Dotted lines* demarcate the boundary of skeletal grainstone intercalation. Diameter of *coin* is 1.5 cm

increase trend (Fig. 11d, e). (2) For the metazoan fossils within microbialites, the correspondence between abundance increase and stratigraphic position is good, with the equation of linear regression being  $y = 0.51x + 1.96$ , correlation coefficient being 0.53 (Fig. 11f). All fossils within microbialites also exhibit a positive correlation with stratigraphic position. Nonetheless, except for worm tubes with a high correlation coefficient (0.46) and obvious increase trend (Fig. 11h), bivalves and brachiopods (coefficient of 0.18), gastropods (coefficient of 0.25), and ostracods (coefficient of 0.13) are not significant in coefficient and increase trend (Fig. 11g, i, j). (3) For the metazoan fossils of skeletal grainstone intercalations, their abundance demonstrates a dramatic positive correlation with the stratigraphic position, with the equation of linear regression being  $y = 6.43x - 52.87$ , correlation coefficient being 0.98 (Fig. 11f), and most taxa, including bivalves and brachiopods (coefficient of 1), worm tubes (coefficient of 0.99),

and ostracods (coefficient of 0.90), also exhibit a prominent increase in trend, and a significant positive correlation with the stratigraphic position (Fig. 11g, h, j), except for gastropods with a relatively weak negative correlation with the stratigraphic position (Fig. 11i).

We also tried to assess each type of metazoan fossil size through the section. However, given the low abundances of worm tubes, gastropods, and ostracods in the mid-lower section (Fig. 4b), errors could occur in the statistics of stratigraphic variation of the fossil sizes due to insufficient specimen. Thus, only the size of bivalves and brachiopods, the abundances and distributions of which are more significant and balanced, are included in the statistical work. We collected 1038 specimen of bivalves and brachiopods in total, and each sample contains more than 40 specimens except for the sample Y-6 with only seven specimens. The MLD (maximum linear dimension) of every specimen was measured and the mid-value in each



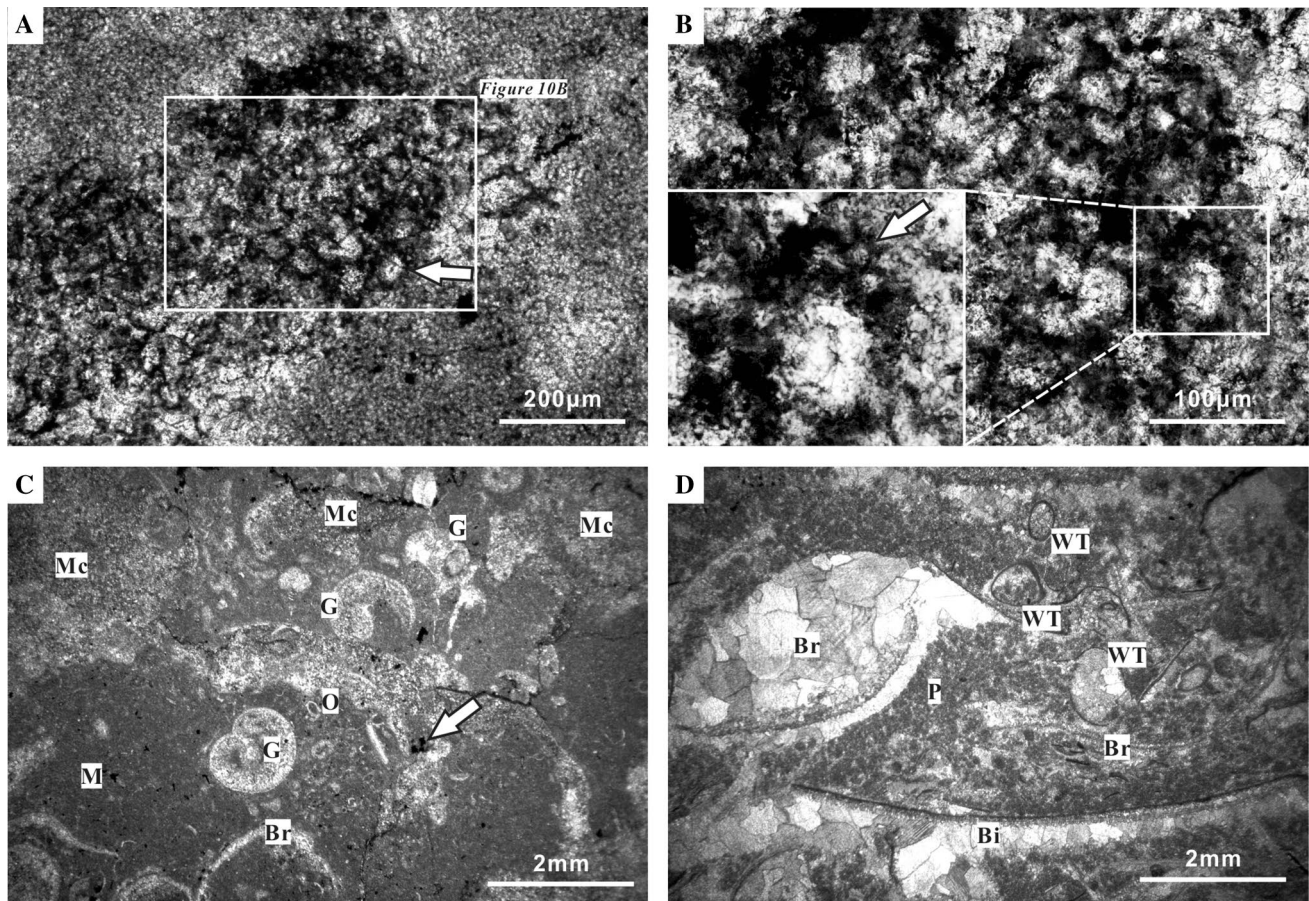


**Fig. 10** **a** Photograph of microstructure of the lamellar-reticular thrombolite. The mesoclot consists mainly of ellipsoidal or capsular small clots (*white arrow*). **b** Close-up of the *rectangle* on **a**. Interior of small clots is filled with spar and hollow coccoidal microbes (*white arrow*) are often mounted in the micrite edges. **c** Spaces between

mesoclots are filled with biotritus, micrite, and rare pyrites (*white arrow*). **d** Within the bioclastic limestone, spaces between bioclastic grains are filled with peloids, and the compacted peloids turned to micrite in places. Abbreviations as in Fig. 4

sample was calculated. The results suggest that the average size of bivalves and brachiopods in each sample varies greatly, with a maximum of 1.29 mm and a minimum of 0.15 mm (Table 2). In order to illustrate the variation in size of bivalves and brachiopods through microbialite beds, box plots of MLD of specimen were developed by using PAST software (Fig. 4c). They demonstrate that: (1) for the overall microbialite deposit, the sizes of bivalve and brachiopod shells generally increase upsection. This is consistent with the results of the correlation analysis; the mid-value of denary logarithm value of MLD of bivalve and brachiopod shells ( $\lg$  (Bi. & Br.)) in each sample demonstrates a high positive correlation with the stratigraphic position, with the equation of linear regression being  $y = 0.06x + 1.22$ , a correlation coefficient of 0.78 (Fig. 11k). (2) For the specimens within microbialites, the increase in size also exists upsection in general terms (Fig. 4c); it is further supported by the significant positive correlation between the mid-value of  $\lg$  (Bi. &

Br.) and the stratigraphic position (Fig. 11l). (3) For the specimens of skeletal grainstone intercalation, there is no obvious increase in shell size through the section, but the mid-values of  $\lg$  (Bi. & Br.) even have a negative correlation with the stratigraphic position (Fig. 11l). However, given the sample Y8-1 contains only three specimens, the trend in size observed here may not be a reliable trend.

In summary, the results above reveal two significant stratigraphic variations in the Yudongzi PTBM succession: (1) the abundance of most metazoan fossils within microbialites increases upsection, and (2) the body size of bivalves and brachiopods generally increases upsection.

### TOC and TS

Measurements of both TOC and TS of the Yudongzi PTBMs yielded low values, with an average value of 0.07 and 0.31 wt%, respectively (Table 3). Also, their maximum values only are 0.20 and 0.66 wt%, respectively (Table 3).

**Table 1** Abundances of metazoan fossils and other fabrics of Yudongzi PTBM succession

Note	Sample no.	Stratigraphic position (m)	Mesoclots (%)	Peloids and (peloidal) micrite (%)	Bivalves and brachiopods (%)	Gastropods (%)	Worm tubes (%)	Ostracoda (%)	Metazoan fossils in total (%)	
The overall microbialite deposit (including microbialites and skeletal grainstone intercalations)	Y12	11.0	0.0	83.0	9.9	0.0	6.4	0.8	17.0	
	Y11	10.6	24.2	67.9	3.5	1.0	2.1	1.3	7.8	
	Y10	10.0	20.6	61.5	8.0	2.4	5.4	2.2	17.9	
	Y9	9.2	36.5	60.4	2.0	0.0	0.8	0.3	3.1	
	Y8	8.9	15.4	69.4	3.6	0.4	11.1	0.2	15.2	
	Y7	8.2	68.8	28.0	1.1	0.3	0.7	1.1	3.2	
	Y6	7.0	69.2	29.4	0.6	0.2	0.4	0.3	1.5	
	Y5	5.1	21.7	71.8	3.9	0.5	0.8	1.4	6.6	
	Y4	3.8	86.0	11.3	1.6	0.5	0.0	0.7	2.7	
	Y3	2.6	28.0	69.5	1.9	0.2	0.0	0.2	2.4	
	Y2	1.3	69.2	26.3	3.6	0.4	0.0	0.5	4.5	
	Y1	0.3	87.8	10.0	0.5	0.1	0.1	1.6	2.2	
	Average			44.0	49.0	3.3	0.5	2.3	0.9	7.0
	Microbialites	Y11	10.6	24.2	67.9	3.5	1.0	2.1	1.3	7.8
		Y10-1	10.0	15.4	75.6	4.1	0.5	2.3	2.1	9.0
Y9		9.2	36.5	60.4	2.0	0.0	0.8	0.3	3.1	
Y8-1		8.9	33.3	54.3	1.0	0.0	11.3	0.2	12.4	
Y7		8.2	68.8	28.0	1.1	0.3	0.7	1.1	3.2	
Y6		7.0	69.2	29.4	0.6	0.2	0.4	0.3	1.5	
Y5		5.1	21.7	71.8	3.9	0.5	0.8	1.4	6.6	
Y4		3.8	86.0	11.3	1.6	0.5	0.0	0.7	2.7	
Skeletal grainstone intercalations	Y3	2.6	28.0	69.5	1.9	0.2	0.0	0.2	2.4	
	Y2	1.3	69.2	26.3	3.6	0.4	0.0	0.5	4.5	
	Y1	0.3	87.8	10.0	0.5	0.1	0.1	1.6	2.2	
	Average			49.1	2.2	0.3	1.7	0.9	5.0	
	Y12	11.0	0.0	83.0	9.9	0.0	6.4	0.8	17.0	
	Y10-2	10.0	0.0	87.1	6.4	2.0	4.4	0.1	12.9	
	Y8-2	8.9	0.0	96.4	2.6	0.6	0.5	0.0	3.6	
	Average			88.8	6.3	0.8	3.8	0.3	11.2	

No. number



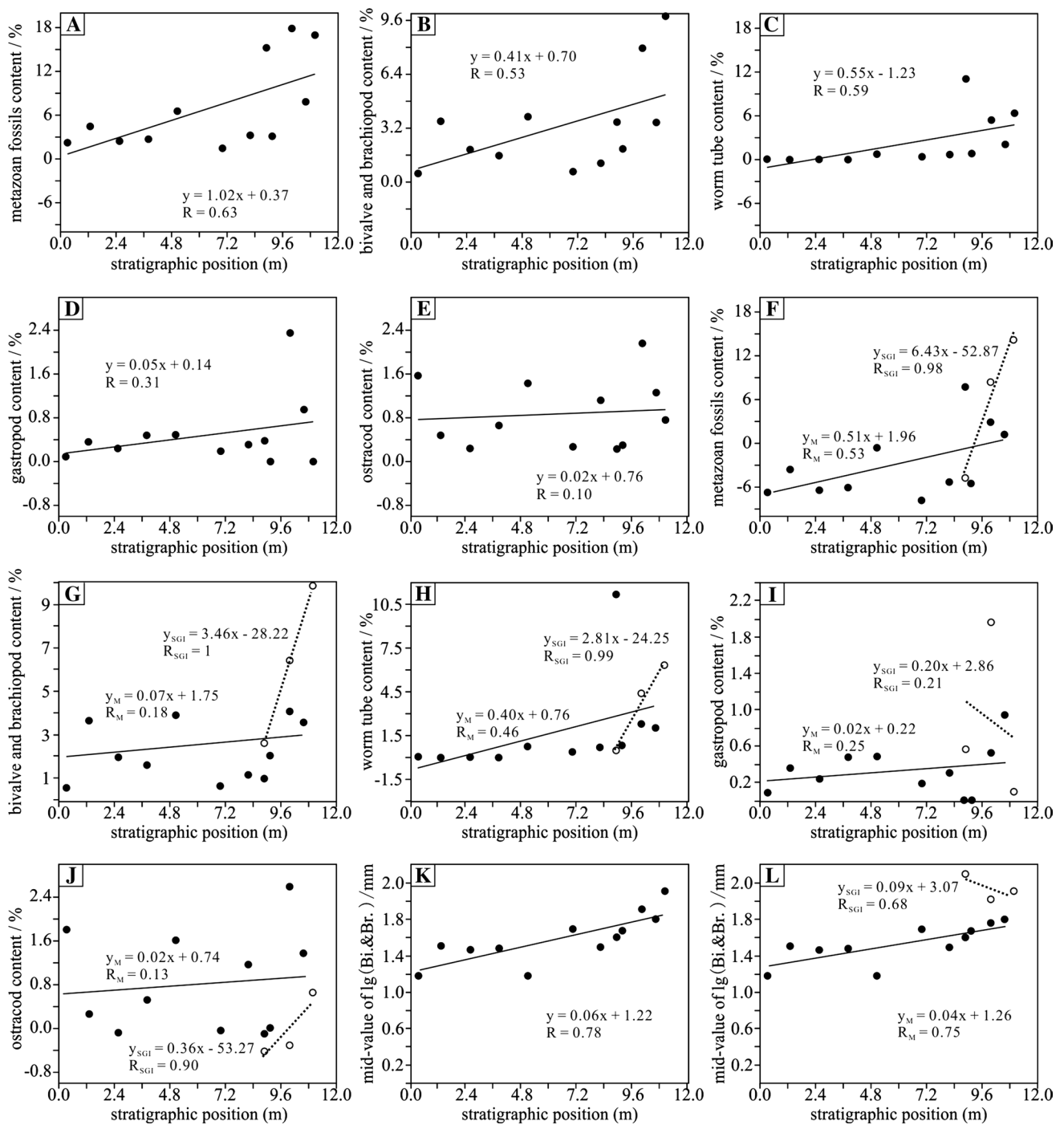


**Fig. 11** Correlation results. **a–e** Correlation analyses between the abundance of metazoan fossils of overall microbialite deposit (including microbialite beds and skeletal grainstone intercalations) and the stratigraphic position. **f–j** Correlation analyses between the fossil

abundance and the stratigraphic position after distinguishing the fossil data inside microbialite beds (solid lines and black dots) from the fossil data in skeletal grainstone intercalations (dotted lines and hollow dots); **a** for the total fossils, **b–e** for the each taxon of total fossils

**Table 2** Data of MLD of bivalves and brachiopods fossils within microbialite beds, skeletal grainstone intercalations, and the overall microbialite deposit

Note	Sample no.	Stratigraphic position (m)	Mid-value (mm)	lg (mid-value) (mm)	Number of specimen ( <i>n</i> )
The overall microbialite deposit (including microbialites and skeletal grainstone intercalations)	Y12	11.0	1.29	2.11	229
	Y11	10.6	0.63	1.80	79
	Y10	10.0	0.81	1.91	73
	Y9	9.2	0.47	1.67	49
	Y8	8.9	0.40	1.60	84
	Y7	8.2	0.31	1.49	69
	Y6	7.0	0.49	1.69	7
	Y5	5.1	0.30	1.18	67
	Y4	3.8	0.15	1.48	112
	Y3	2.6	0.29	1.46	47
	Y2	1.3	0.32	1.51	94
	Y1	0.3	0.15	1.18	128
Microbialites	Y11	10.6	0.63	1.80	79
	Y10-1	10.0	0.57	1.76	41
	Y9	9.2	0.47	1.67	49
	Y8-1	8.9	0.39	1.59	81
	Y7	8.2	0.31	1.49	69
	Y6	7.0	0.49	1.69	7
	Y5	5.1	0.30	1.18	67
	Y4	3.8	0.15	1.48	112
	Y3	2.6	0.29	1.46	47
	Y2	1.3	0.32	1.51	94
Skeletal grainstone intercalations	Y1	0.3	0.15	1.18	128
	Y12	11.0	1.29	2.11	229
	Y10-2	10.0	1.06	2.02	32
	Y8-2	8.9	2.30	2.03	3

No. number

**Table 3** Abundances of TOC and TS of the Yudongzi PTBMs

Sample no.	Stratigraphic position (m)	TOC (wt%)	TS (wt%)
Y12	11.0	0.06	0.09
Y11	10.6	0.04	0.48
Y10	10.0	0.08	0.27
Y9	9.2	0.05	0.66
Y8	8.9	0.20	0.18
Y7	8.2	0.07	0.37
Y6	7.0	0.06	0.28
Y5	5.1	0.04	0.57
Y4	3.8	0.11	0.24
Y3	2.6	0.05	0.32
Y2	1.3	0.06	0.18
Y1	0.3	0.03	0.07
Average		0.07	0.31

No. number, TOC total organic carbon, TS total sulfur

## Discussion

### Implications of stratigraphic variations in the PTBM succession

Oxygen may have played an important role in the process of the increase in abundance and size of metazoa of marine settings. Payne et al. (2006) documented variations in the abundance and diversity of fossils from end-Permian to Middle Triassic on the Great Guizhou Bank using microfacies analysis and point counting. In the Griesbachian, they found that the platform interior contains evidence for metazoan life while the deeper-water facies (platform margin and basin margin) were totally depauperate. Pietsch and Bottjer (2014) suggested that this pattern is due to deeper environments with low oxygen or anoxic condition at this time. Song et al. (2012) interpreted increase in Ce and Th/U represent

a widespread, potentially global, low-oxygen event from the end-Permian through the Griesbachian and possibly the early Dienerian. Also, as the global low-oxygen conditions ameliorated through the interval following end-Spathian (Song et al. 2012), the abundance of metazoa increased significantly in both platform margin and basin margin environment, but hardly changed in the platform interior due to the poor aeration and insufficient oxygen in restricted environment (Payne et al. 2006; Pietsch and Bottjer 2014). These interpretations support the view that there was good correspondence between metazoan abundance increase and oxic seawater. Thus, the increase in abundance of metazoan fossils through the Yudongzi PTBM succession may suggest the microbialite grew in oxic seawater. Further support comes from the work of Hautmann et al. (2011, 2015) describing rich shelly faunas from microbialites elsewhere in the South China sequences, and their work seems to demonstrate that the poor development of shelly faunas in most PTBMs is not uniform. Whether this relates to regional variation in oxygenation or possibly variations in preservation of fossils cannot be assessed in our study, but do show that the results across the end-Permian event are not the same everywhere.

Metazoan body size also has a significant link with the oxygen concentration in the marine environment according to a large number of published studies. Rhoads and Morse (1971) and Savrda et al. (1984) demonstrated that benthonic animals in the Gulf of California and other places had a reduction in body size due to oxygen deficiency, indicating the size of benthonic organisms was subject to oxygen content in the environment. Oschmann (1993) argued that for the adaption to shallow seawater with low-oxygen values, the benthonic animals can evolve from the normal pelago-benthic (planktotrophic larvae, benthic adults) to the progenetic holo-pelagic (planktotrophic larvae, planktic adults) life cycle by a delay of somatic development as well as by early sexual maturity, which lead to the reduction in the body size of benthos. This view was further supported by recent experimental data, which generally shows that animals reach smaller maximum adult size and/or mature at smaller size under conditions of sub-lethal hypoxia (Richmond et al. 2006). On the contrary, in well-oxygenated conditions, such as in Oman, the sizes of shelly taxa are larger than the localities of identical age with low-oxygen conditions (Wheelely and Twitchett 2005). Thus, from these studies, the correspondence between benthic body size and oxygenation condition of seawater is good, suggesting that the increase in body size of bivalves and brachiopods, together with increase in abundance, maybe represent the amelioration of redox conditions or relatively sufficient oxygen content during the Yudongzi microbialites growth.

We interpret the evidence from Yudongzi as indicating well-oxygenated conditions in the microbialite, but there is evidence from other sites across the Permian–Triassic

extinction interval of varying oxygen conditions. In deeper waters, Grasby et al. (2013) interpreted distal slope marine anoxia repeatedly affected the area now occupied by the Sverdrup Basin, through the 5 million year recovery phase after the extinction. In the deep shelf site at Shangsi, Sichuan Province, China, Xiang et al. (2016) demonstrated fluctuations of oxygenation that started in the Late Permian with euxinic conditions, but through the extinction strata there was fluctuation of oxic to anoxic waters. Loope et al. (2013) interpreted oxic conditions in shallow waters at Demirtas in Turkey and Cili in south China, thus showing consistency with our results. However, in contrast, in the boreal realm in what is now Spitsbergen, in clastic facies that lack microbialites, Wignall et al. (2015) identified anoxia in very shallow waters, noting that they showed fluctuations that they suggested may have been due to climatic oscillations. New work by Wang et al. (2016) reinterpreted Cili PTBMs (China) to form in dysoxic conditions based on pyrite framboids data, which is different from Loope et al. (2013) but consistent with Liao et al. (2010).

#### Chemical indicators of redox condition of the PTBMs

In anoxic settings, the limitation of aerobic decomposers normally lead to organic carbon contents increasing (e.g., Arthur and Sageman 1994), also sulfides contents trend to increase due to metabolism of sulfate reducers (e.g., Berner 1970). Therefore, TOC and TS contents can be used as indicators of redox condition in some cases (e.g., Marengo et al. 2012, 2013). Comparing with the compiled data of representative researches that include assessment of redox condition, we found that TOC and TS contents of Yudongzi PTBMs are very low (Table 4); The average values of TOC and TS of rocks in Majiashan (9.41 wt% TOC, 5.22 wt% TS), Changqiao (6.22 wt% TOC, 2 wt% TS) and Shangsi (3.17 wt% TOC), which are interpreted to deposit in anoxic seawater according to the ratios of V/(V + Ni), V/Cr, Ni/Co, and U/Th (Xie et al. 2008; Chen et al. 2013), are considerably higher than our results (0.07 wt% TOC, 0.31 wt% TS) (Table 4). On the contrary, the rather low average values of TOC and TS of this study are similar to the data from Fossil Mountain (0.2 wt% TOC, 0.02 wt% TS) and Lost Cabin Spring (0.2 wt% TOC, 0.02 wt% TS), where it has been considered that the anoxia was not prevalent in depositional environments (Marengo et al. 2012, 2013).

Thus, it appears to indicate that environmental settings were oxic during Yudongzi PTBMs deposition. However, the low TOC and TS values can be interpreted in multiple ways (Marengo et al. 2013). We thus further considered other possibilities as follows: (1) low production of organic carbon could result in low TOC abundances (e.g., Shen et al. 2015). Nevertheless, microbial mats can accumulate significant amounts of organic matter due to the abundant bacterial



**Table 4** TOC and TS abundances of several representative studies, which also did a detailed assessment of redox condition

Seawater redox condition	Location	Rock	TOC	TS	Criteria of redox condition
Anoxic	Majiashan, Anhui, China (Chen et al. 2013)	Carbonaceous and siliceous shales of Upper Permian Dalong Formation	5 to 14.3 wt%, 9.41 wt% on average	2 to 10 wt%, 5.22 wt% on average	V/(V + Ni); V/Cr; Ni/Co; U/Th
	Changqiao, Anhui, China (Chen et al. 2013)	Carbonaceous and siliceous shales of Upper Permian Dalong Formation	2.5 to 11.8 wt%, 6.22 wt% on average	0 to 5 wt%, 2 wt% on average	V/(V + Ni); V/Cr; Ni/Co; U/Th
	Shangsi, Sichuan, China (Xie et al. 2008)	Calcareous mudstones, laminated marls and thin-bedded limestones of Upper Permian Dalong Formation	0.25 to 13.8 wt%, 3.17 wt% on average		Ni/(Ni + V); V/Cr; Ni/Co
Oxic	Fossil Mountain, Utah, USA (Marenco et al. 2012)	Limestone and sandy limestone of Middle Ordovician Juab Formation and Kanosh Formation	0 to 0.8 wt%, 0.2 wt% on average	0 to 0.07 wt%, 0.02 wt% on average	TOC and TS, and other ecological evidences such the present of burrows and sponges
	Lost Cabin Spring, Nevada, USA (Marenco et al. 2013)	Fossiliferous limestone, calcareous siltstone, and interbedded carbonate and siltstone of Lower Triassic Virgin Limestone	0 to 0.6 wt%, 0.2 wt% on average	0.01 to 0.09 wt%, 0.02 wt% on average	TOC and TS

No. number, TOC total organic carbon, TS total sulfur

communities (Dupraz et al. 2009). Microbial mat-dwelling organisms, and planktic communities consisting mainly of bacteria (Luo et al. 2013) should provide abundant organic sources as well. Notably, mesoclots and peloids, as aggregations of microbes (Adachi et al. 2004), should be robust potential organic sources due to their significant abundances. (2) The sedimentation rate is often negatively related to the TOC abundance (e.g., Xie et al. 2008; Li et al. 2011). Li et al. (2011) quantitatively calculated the approximate sedimentation rates of Dalong Formation and Wujiaping Formation of Shangsi, revealing that the former, with slow sedimentation (3.98 cm/ka in upper parts, 2.18 cm/ka in lower parts), has high TOC values (2.2 wt% in upper parts, 5.6 wt% in lower parts) while the latter depositing quickly (5.08 cm/ka) contains low TOC abundance (0.87 wt%). We calculated the sedimentation rate of Yudongzi PTBMs to be ca. 2.75 cm/ka, based on the thickness of microbialites (ca. 11 m) and the duration of *Hindeodus parvus* Zone (ca. 0.4 Ma) (Ogg 2012). This is a low average value (noting that the numerous small erosion surfaces in the microbialite likely mean the actual accumulation rates were higher), like the Dalong Formation, but did not yield high TOC values, suggesting the possibility of oxic depositional environments or other alternative interpretations. (3) Organic mass could have been reduced due to thermal maturation during burial. However, the Dalong Formation of Shangsi, which has a similar burial depth and history to the Yudongzi PTBMs (Wang 1989), is considered to have low maturity in organic matter according to the low bitumen reflectance (merely 0.69%) (Fu et al. 2010), indicating only little organic matter could be decomposed in microbialites. Zhong et al. (2004) even argue that the natural process of hydrocarbon generation and expulsion does not change TOC values noticeably based on their simulation experiments. (4) Due to the lack of sulfate-bearing minerals revealed in petrographic results, TS values are assumed to reflect pyrite content. Thus, the low TS values could be the result of low organic production or iron limitation (Marenco et al. 2013). However, the organic production is not likely low as the above discussed. As to the iron limitation, surrounding uplifts such as Khamdian (Fig. 1d) should have been able to provide sufficient available iron to the Yangtze area through clastic input from weathering. This is supported by the prevalence of pyrite in the Dalong Formation. Therefore, as discussed above, the low TOC and TS values of this study most likely indicate an oxic depositional environment during the Yudongzi microbialites growth, resulting in poor preservation of organic matter and limitation of bacterial sulfate reduction.

### Paleoenvironmental significance of the PTBMs

To emphasize the contrast between our new results and previous interpretations, we note some key features of

previous ideas. PTBMs were initially considered disaster forms (e.g., Kershaw et al. 1999; Lehrmann 1999; Lehrmann et al. 2001) similar to the Spathian microbialites in United States (cf. Schubert and Bottjer 1992). Understanding of PTBMs, however, has gradually changed as with more comprehensive studies of major geological events during the Permian–Triassic boundary interval and of special marine structures. Grotzinger and Knoll (1995) considered that the abundant anomalous carbonate precipitates in late Permian reefs might be the result of supersaturation as anoxic deep seawaters enriched in carbonate alkalinity upwelled to oxic surface seawater. Knoll et al. (1996) further proposed the hypothesis that the overturn of anoxic deep oceans during the Late Permian introduced high concentrations of CO<sub>2</sub> into surficial environments and caused the end-Permian mass extinction, which was supported later by the mode of “Stratified Superocean” developed by Isozaki (1997). Inspired by the above, Kershaw et al. (1999) proposed the upwelling model to interpret the formation of PTBMs. According to the process envisaged, organic matter concentrated in anoxic stratified ocean bottom was subject to sulfate reduction under the effect of anaerobic bacteria, presumed to have given rise to a large reservoir of dissolved inorganic carbon (DIC) present as HCO<sub>3</sub><sup>-</sup>, CO<sub>3</sub><sup>2-</sup>, together with H<sub>2</sub>S. The DIC was upwelled to oxygen-enriched shallow sea and quickly degassed, resulting in extreme saturation of the carbonate content of the seawater so that calcification of microbial mats and the formation of PTBMs took place. This model was widely invoked in numerous studies (Lehrmann et al. 2003; Baud et al. 2005, 2007; Hips and Haas 2006; Pruss et al. 2006; Kershaw et al. 2007; Ezaki et al. 2008; Kershaw et al. 2009, 2011; Mary and Woods 2008; Mata and Bottjer 2011). Coupling between PTBMs occurrence and the negative excursion of carbon isotopes (Mu et al. 2009) supported this hypothesis. However, despite these points, Kershaw et al. (2012) proposed that there is a problem with the upwelling model because the Permian reefs (directly underlying extinction facies) contain abundant cements and hypercalcifier skeletal fossils. Not only do these fossils disappear with the extinction, making carbonate available to the environment, but also the PTBMs do not contain extensive inorganic carbonate cements. These observations imply that carbonate saturation was not necessarily increased after the extinction, so that increased saturation may not necessarily be the driver of microbialite growth after the extinction. Furthermore, the upwelling model includes input of H<sub>2</sub>S from the deep ocean, mentioned above; it may be argued that such input could reduce ocean pH further, which would act to inhibit CaCO<sub>3</sub> precipitation. The presence of the microbialites, as deposited carbonate, thus seems to reduce the likelihood of substantial H<sub>2</sub>S input to the area of microbialite formation, but this does not necessarily mean the H<sub>2</sub>S was not part of the system.

This idea has not yet been explored in further detail and will be tested as the database on PTBMs grows. Recently, Lehrmann et al. (2015) also questioned the upwelling model due to relatively uniform thickness of PTBMs on isolated carbonate platforms of Nanpanjiang basin.

Another key aspect is anoxia. The delayed biotic recovery from the end-Permian mass extinction has been considered to be caused by anoxic seawater with high concentrations of CO<sub>2</sub> (Twitchett et al. 2004; Fraiser and Bottjer 2007), therefore, PTBMs have been also associated with the Early Triassic anomalous marine environment (e.g., Pruss and Bottjer 2004; Knoll et al. 2007) and regarded as an indicator of harsh environment impeding the recovery (e.g., Mary and Woods 2008). Schobben et al. (2015) showed extensive reduction of oxygen contents in the sea water on deeper parts of carbonate platforms and stated that poor conditions continued through the Early Triassic. PTBMs only have a very small stratigraphic distribution so that they cannot match the continuing poor deeper-shelf conditions; if they are directly related to the deeper-shelf anoxia, we would expect to see PTBMs persisting in the whole Early Triassic time. An alternative interpretation is that PTBMs are facies controlled and therefore only develop in shallow waters (Kershaw et al. 2012); when sea level rose in the Early Triassic, the environment was not suitable for microbialite-forming microbial mats, even if deeper anoxic water continued to upwell. However, we would expect to see the microbialites in near-shore areas, as sea level rose, but there appear to be no examples reported so far, instead the microbialites disappeared. Thus we suggest the environment of PTBMs was not directly related to the deeper shelf anoxia. In addition, the diameter of pyrite framboids in the PTBMs (Liao et al. 2010 and papers cited within) was used to suggest low oxygen conditions in recent years, but the conflict between pyrite framboid data and the presence of ostracods and gastropods in the microbialite led Kershaw (2015) to propose the possibility that framboids were imported into the microbialite by currents, using data and processes known from the modern Black Sea, thus disturbing the signal of pyrite as an indicator of low oxygen, previously considered to be a robust proxy. Our data presented in this paper suggest that the microbialites formed in oxygenated conditions. For the reason of oxygenation, Forel et al. (2013) suggested photosynthesis in the microbialites provided a local oxygen refuge while the anoxic upwelling had occurred yet in otherwise zones. However, it seems to be not matched by the TOC and TS data presented here because the abundance of total organic matter and sulfur would tend to increase when the microbialites died in persistent anoxic upwelling zones. Pietsch and Bottjer (2014) recently showed that “shortly after the extinction event, shoreface environments with moderate wave energy were sites of water column oxygenation that supported a

more rapid return to diverse and ecologically complex benthic communities.” Skeletal intercalations and the occurrence on the top of Permian reef indicate that Yudongzi PTBMs may have developed in very shallow environments, like other subtidal microbialites in China (Lehrmann et al. 2003; Kershaw et al. 2012). Thus the oxygenation of their depositional environments may well be related to the mixing of ocean surface waters in contact with the atmosphere.

## Conclusions

This paper documents a new PTBM section located in the Yudongzi area near Erlangmiao Town, in the district of Jiangyou City, northwestern Sichuan Basin of China from the north margin of Upper Yangtze platform. These microbialites occur mainly in the *Hindeodus parvus* Zone but may cross the Permian–Triassic boundary, according to the conodont biostratigraphy of the Yudongzi section. They are up to ca. 11 m in thickness and comprised of, from bottom to top: lamellar thrombolites, dendritic thrombolites and lamellar-reticular thrombolites. Statistical calculations reveal that most metazoan fossils within microbialites increase in abundance upsection, so does the sizes of bivalve and brachiopod fossils. Also, we measured TOC and TS values of microbialites, both of which are very low, accounting respectively for 0.07 and 0.31 wt% on average.

In contrast to the established interpretations of PTBM environmental conditions, the new results presented in this paper indicate that the ancient ambient seawater was oxic during the growth of PTBMs at the Yudongzi site, based on the analyses of stratigraphic variations in fossils in the succession and low TOC and TS contents of the microbialite. Given the overall similarity between microbialites at Yudongzi and other PTBM sites in China, we thus dispute the previous view, at least for the Chinese sequences, of low oxygen seawater for microbialite growth, and question whether it is now appropriate to associate PTBMs with anoxic, harsh environments associated with the end-Permian extinction. Instead we interpret those conditions as fully oxygenated.

**Acknowledgements** We are grateful to Prof. Jindong Xiao of China University of Geosciences (CUG) for his assistance in the field, and revision of an early version of this paper. We also thank Pedro Marengo of Bryn Mawr College for his advice about TOC and TS analyses; Haishui Jiang of CUG for the identification of conodonts; Qiye Zhang of Southwest Petroleum University for his statistical works in this paper; and Jeong-Hyun Lee of Seoul National University for valuable discussion. We thank Wolfgang Kiessling, Jörn Peckmann, and an anonymous reviewer for their valuable comments, improving the paper. This work was supported by the 13th Five-Year Plan National Scientific and Technology Major Project (2016ZX05004002-001), and National Natural Science Foundation of China (41602166).



**Open Access** This article is distributed under the terms of the Creative Commons Attribution 4.0 International License (<http://creativecommons.org/licenses/by/4.0/>), which permits unrestricted use, distribution, and reproduction in any medium, provided you give appropriate credit to the original author(s) and the source, provide a link to the Creative Commons license, and indicate if changes were made.

## References

- Adachi N, Ezaki Y, Liu J (2004) The fabrics and origins of peloids immediately after the end-Permian extinction, Guizhou Province, South China. *Sed Geol* 164:161–178
- Arthur MA, Sageman BB (1994) Marine shales: depositional mechanisms and environments of ancient deposits. *Annu Rev Earth Planet Sci* 22:499–551
- Baud A, Richoz S, Marcoux J (2005) Calcimicrobial cap rocks from the basal Triassic units: western Taurus occurrences (SW Turkey). *CR Palevol* 4(6):569–582
- Baud A, Richoz S, Pruss S (2007) The lower Triassic anachronistic carbonate facies in space and time. *Global Planet Change* 55(1–3):81–89
- Berner RA (1970) Sedimentary pyrite formation. *Am J Sci* 268(1):1–23
- Chen P, Zhang M, Xu Y, Liu J, Du X, Hu X, Lu Y (2013) The shale reservoir characteristic of Dalong Formation Upper Permian in Chaohu-Jingxian, Lower Yangtze area. *Acta Petrol Sin* 29(8):2925–2935 (in Chinese with English abstract)
- Chen ZQ, Wang Y, Kershaw S, Luo M, Yang H, Zhao L, Feng Y, Chen J, Yang L, Zhang L (2014) Early Triassic stromatolites in a siliciclastic nearshore setting in northern Perth Basin, Western Australia: geobiologic features and implications for post-extinction microbial proliferation. *Global Planet Change* 121:89–100
- Collin PY, Kershaw S, Tribouvillard N, Forel MB, Crasquin S (2014) Geochemistry of post-extinction microbialites as a powerful tool to assess the oxygenation of shallow marine water in the immediate aftermath of the end-Permian mass extinction. *Int J Earth Sci* 104(4):1025–1037
- Dupraz C, Reid RP, Braissant O, Decho AW, Norman RS, Visscher PT (2009) Processes of carbonate precipitation in modern microbial mats. *Earth Sci Rev* 96(3):141–162
- Ezaki Y, Liu J, Adachi N (2003) Earliest Triassic microbialite micro-to megastructures in the Huaying area of Sichuan Province, South China: implications for the nature of oceanic conditions after the end-Permian extinction. *Palaios* 18:388–402
- Ezaki Y, Liu J, Nagano T, Adachi N (2008) Geobiological aspects of the earliest Triassic microbialites along the southern periphery of the tropical Yangtze platform: initiation and cessation of a microbial regime. *Palaios* 23(6):356–369
- Forel MB, Crasquin S, Kershaw S, Collin PY (2013) In the aftermath of the end-Permian extinction: the microbialite refuge? *Terra Nova* 25(2):137–143
- Fraiser ML, Bottjer DJ (2007) Elevated atmospheric CO<sub>2</sub> and the delayed biotic recovery from the end-Permian mass extinction. *Palaeogeogr Palaeoclimatol Palaeoecol* 252(1–2):164–175
- Fu X, Qin J, Tenger, Wang X (2010) Evaluation on Dalong formation source rock in the North Sichuan Basin. *Pet Geol Exp* 32(6):566–577 (in Chinese with English abstract)
- Grasby SE, Sanei H, Beauchamp B, Chen Z (2013) Mercury deposition through the Permo–Triassic biotic crisis. *Chem Geol* 351:209–216
- Grotzinger JP, Knoll AH (1995) Anomalous carbonate precipitates: is the Precambrian the key to the Permian. *Palaios* 10:578–596
- Hammer Ø, Harper DAT, Ryan PD (2001) Past: paleontological statistics software package for education and data analysis. *Palaeontol Electron* 4(1):1–9
- Hautmann M, Bucher H, Brühwiler T, Goudemand N, Kaim A, Nützel A (2011) An unusually diverse mollusc fauna from the earliest Triassic of South China and its implications for benthic recovery after the end-Permian biotic crisis. *Geobios* 44:71–85
- Hautmann M, Bagherpour B, Brosse M, Frisk Å, Hofmann R, Baud A, Bucher H (2015) Competition in slow motion: the unusual case of benthic marine communities in the wake of the end-Permian mass extinction. *Palaeontology* 58(5):871–901
- He L, Wang Y, Woods A, Li G, Yang H, Liao W (2013) Calcareous tubeworms as disaster forms after the end-Permian mass extinction in South China. *Palaios* 27(12):878–886
- He J, Zheng R, Hu X, Zhang B, Yin H, Ma H, Wang Y, Feng C (2015) Sedimentary system of the Late Permian Wujiaping formation in the western Sichuan Basin. *Oil Gas Geol* 36(1):87–95 (in Chinese with English abstract)
- Hips K, Haas J (2006) Calcimicrobial stromatolites at the Permian–Triassic boundary in a western Tethyan section, Bükk Mountains, Hungary. *Sediment Geol* 185(3–4):239–253
- Isozaki Y (1997) Permo–Triassic boundary superanoxia and stratified superocean: records from lost deep sea. *Science* 276(5310):235–238
- Jiang H, Lai X, Luo G, Aldridge R, Zhang K, Wignall P (2007) Restudy of conodont zonation and evolution across the P/T boundary at Meishan section, Changxing, Zhejiang, China. *Global Planet Change* 55(1–3):39–55
- Jiang H, Lai X, Sun Y, Wignall P, Liu J, Yan C (2014) Permian–Triassic conodonts from Dajiang (Guizhou, South China) and their implication for the age of microbialite deposition in the aftermath of the end-Permian mass extinction. *J Earth Sci* 25(3):413–430
- Kershaw S (2015) Modern Black Sea oceanography applied to the end-Permian extinction event. *J Palaeogeogr* 4(1):52–62
- Kershaw S, Zhang T, Lan G (1999) A ? microbialite carbonate crust at the Permian–Triassic boundary in South China, and its palaeoenvironmental significance. *Palaeogeogr Palaeoclimatol Palaeoecol* 146:1–18
- Kershaw S, Guo L, Swift A, Fan J (2002) ?Microbialites in the Permian–Triassic boundary interval in central China: structure, age and distribution. *Facies* 47:83–90
- Kershaw S, Li Y, Crasquin-Soleau S, Feng Q, Mu X, Collin PY, Reynolds A, Guo L (2007) Earliest Triassic microbialites in the South China block and other areas: controls on their growth and distribution. *Facies* 53(3):409–425
- Kershaw S, Crasquin S, Collin PY, Li Y, Feng Q, Forel MB (2009) Microbialites as disaster forms in anachronistic facies following the end-Permian mass extinction: a discussion. *Aust J Earth Sci* 56(6):809–813
- Kershaw S, Crasquin S, Forel MB, Randon C, Collin PY, Kosun E, Richoz S, Baud A (2011) Earliest Triassic microbialites in Çürük Dag, southern Turkey: composition, sequences and controls on formation. *Sedimentology* 58(3):739–755
- Kershaw S, Crasquin S, Li Y, Collin PY, Forel MB, Mu X, Baud A, Wang Y, Xie S, Maurer F, Guo L (2012) Microbialites and global environmental change across the Permian–Triassic boundary: a synthesis. *Geobiology* 10(1):25–47
- Knoll AH, Bambach RK, Canfield DE, Grotzinger JP (1996) Comparative earth history and late Permian Mass extinction. *Science* 273(5274):452–457
- Knoll AH, Bambach RK, Payne JL, Pruss S, Fischer WW (2007) Paleophysiology and end-Permian mass extinction. *Earth Planet Sci Lett* 256(3):295–313

- Lehrmann DJ (1999) Early Triassic calcimicrobial mounds and biostromes of the Nanpanjiang basin, south China. *Geology* 27(4):359–362
- Lehrmann DJ, Wan Y, Wei J, Yu Y, Xiao J (2001) Low Triassic peritidal cyclic limestone: an example of anachronistic carbonate facies from the Great Bank of Guizhou, Nanpanjiang Basin, Guizhou province, South China. *Palaeogeogr Palaeoclimatol Palaeoecol* 173:103–123
- Lehrmann DJ, Payne J, Felix S, Dillett PM, Wang H, Yu Y, Wei J (2003) Permian–Triassic boundary sections from shallow-marine carbonate platforms of the Nanpanjiang Basin, South China: implications for oceanic conditions associated with the end-Permian extinction and its aftermath. *Palaios* 18:138–152
- Lehrmann DJ, Bentz JM, Wood T, Goers A, Dhillon R, Akin S, Li X, Payne JL, Kelley BM, Meyer KM, Schaal EK, Suarez MB, Yu M, Qin Y, Li R, Minzoni M, Henderson CM (2015) Environmental controls on the genesis of marine microbialites and dissolution surface associated with the end-Permian mass extinction: new sections and observations from the Nanpanjiang Basin, South China. *Palaios* 30(7):529–552
- Li N, Hu C, Ma Z, Yan J (2011) Main control factors of high quality hydrocarbon source rocks of the Upper Permian Dalong Formation at Shangsi section of Guangyuan, Sichuan Province. *J Palaeogeogr* 13(3):347–354 (in Chinese with English abstract)
- Liao W, Wang Y, Kershaw S, Weng Z, Yang H (2010) Shallow-marine dysoxia across the Permian–Triassic boundary: evidence from pyrite framboids in the microbialite in South China. *Sed Geol* 232(1–2):77–83
- Liu H, Wang Y, Yuan A, Yang H, Song H, Zhang S (2010) Ostracod fauna across the Permian–Triassic boundary at Chongyang, Hubei Province, and its implication for the process of the mass extinction. *Sci China Earth Sci* 53(6):810–817
- Liu L, Jiang H, Wu Y, Cai C (2014) Community replacement sequences and paleoenvironmental changes in reef areas of South China from Late Permian to Early Triassic exemplified by Panlongdong section in northeastern Sichuan Basin. *Sci China Earth Sci* 57(5):1093–1108
- Loope GR, Kump LR, Arthur MA (2013) Shallow water redox conditions from the Permian–Triassic boundary microbialite: the rare earth element and iodine geochemistry of carbonates from Turkey and South China. *Chem Geol* 351:195–208
- Luo G, Wang Y, Grice K, Kershaw S, Algeo TJ, Ruan X, Yang H, Jia C, Xie S (2013) Microbial–algal community changes during the latest Permian ecological crisis: evidence from lipid biomarkers at Cili, South China. *Global Planet Change* 105:36–51
- Marengo PJ, Griffin JM, Fraiser ML, Clapham ME (2012) Paleogeology and geochemistry of Early Triassic (Spathian) microbial mounds and implications for anoxia following the end-Permian mass extinction. *Geology* 40(8):715–718
- Marengo PJ, Marengo KN, Lubitz RL, Niu D (2013) Contrasting long-term global and short-term local redox proxies during the Great Ordovician Biodiversification Event: a case study from Fossil Mountain, Utah, USA. *Palaeogeogr Palaeoclimatol Palaeoecol* 377:45–51
- Mary M, Woods AD (2008) Stromatolites of the Lower Triassic Union Wash Formation, CA: evidence for continued post-extinction environmental stress in western North America through the Spathian. *Palaeogeogr Palaeoclimatol Palaeoecol* 261(1–2):78–86
- Mata SA, Bottjer DJ (2011) Origin of Lower Triassic microbialites in mixed carbonate-siliciclastic successions: ichnology, applied stratigraphy, and the end-Permian mass extinction. *Palaeogeogr Palaeoclimatol Palaeoecol* 300(1–4):158–178
- Mu X, Kershaw S, Li Y, Guo L, Qi Y, Reynolds A (2009) High-resolution carbon isotope changes in the Permian–Triassic boundary interval, Chongqing, South China; implications for control and growth of earliest Triassic microbialites. *J Asian Earth Sci* 36(6):434–441
- Novack-Gottshall PM (2008) Using simple body-size metrics to estimate fossil body volume: empirical validation using diverse Paleozoic invertebrates. *Palaios* 23(3):163–173
- Ogg JG (2012) Triassic. In: Gradstein FM, Ogg JG, Schmitz M, Ogg G (eds) *The geologic time scale 2012*. Elsevier, Amsterdam, pp 680–730
- Oschmann W (1993) Environment oxygen fluctuations and the adaptive response of marine benthic organisms. *J Geol Soc* 150(1):187–191
- Payne JL, Lehrmann DJ, Wei J, Knoll AH (2006) The pattern and timing of biotic recovery from the end-Permian extinction on the Great Bank of Guizhou, Guizhou Province, China. *Palaios* 21(1):63–85
- Pietsch C, Bottjer DJ (2014) The importance of oxygen for the disparate recovery patterns of the benthic macrofauna in the Early Triassic. *Earth Sci Rev* 137:65–84
- Pruss SB, Bottjer DJ (2004) Late Early Triassic microbial reefs of the western United States: a description and model for their deposition in the aftermath of the end-Permian mass extinction. *Palaeogeogr Palaeoclimatol Palaeoecol* 211(1–2):127–137
- Pruss SB, Corsetti FA, Bottjer DJ (2005) The unusual sedimentary rock record of the Early Triassic: a case study from the southwestern United States. *Palaeogeogr Palaeoclimatol Palaeoecol* 222(1–2):22–52
- Pruss SB, Bottjer DJ, Corsetti FA, Baud A (2006) A global marine sedimentary response to the end-Permian mass extinction: examples from southern Turkey and the western United States. *Earth Sci Rev* 78(3–4):193–206
- Rhoads DC, Morse JW (1971) Evolutionary and ecologic significance of oxygen-deficient marine basins. *Lethaia* 4(4):413–428
- Richmond C, Marcus NH, Sedlacek C, Miller GA, Oppert C (2006) Hypoxia and seasonal temperature: short-term effects and long-term implications for *Acartia tonsa* dana. *J Exp Mar Biol Ecol* 328(2):177–196
- Rong H, Jiao Y, Wu L, Li R, Wang R, Wang S, Yang S (2009) Organic bioherms and their forming models of Changxing formation in Manyue-Ganquan section of Kaixian, Northeast Sichuan. *Acta Sedimentol Sin* 27(1):9–17 (in Chinese with English abstract)
- Rong H, Jiao Y, Wu L, Gu Y, Zhang L (2012) Relationship between heterogeneity and seismic velocities of the Yudongzi Triassic oolitic reservoirs in the Erlangmiao area, northwest Sichuan Basin, China. *J Petrol Sci Eng* 100:81–98
- Savrdra CE, Bottjer DJ, Gorsline DS (1984) Development of a comprehensive oxygen-deficient marine biofacies model: evidence from Santa Monica, San Pedro, and Santa Barbara Basins, California Continental Borderland. *AAPG Bull* 68(9):1179–1192
- Schobben M, Stebbins A, Ghaderi A, Strauss H, Korn D, Korte C (2015) Flourishing ocean drives the end-Permian marine mass extinction. *Proc Natl Acad Sci USA* 112(33):10298–10303
- Schubert JK, Bottjer DJ (1992) Early Triassic stromatolites as post-mass extinction disaster forms. *Geology* 20(10):883–886
- Sepkoski JJ, Bambach R, Droser M (1991) Secular changes in Phanerozoic event bedding and the biological overprint. In: Einsele G, Ricken W, Seilacher A (eds) *Cycles and events in stratigraphy*. Springer, Berlin, pp 298–312
- Shapiro RS (2000) A comment on the systematic confusion of thrombolites. *Palaios* 15(2):166–169
- Shen J, Schoepfer SD, Feng Q, Zhou L, Yu J, Song H, Wei H, Algeo TJ (2015) Marine productivity changes during the end-Permian crisis and Early Triassic recovery. *Earth Sci Rev* 149:136–162
- Song H, Wignall PB, Tong J, Bond DPG, Song H, Lai X, Zhang K, Wang H, Chen Y (2012) Geochemical evidence from bioapatite for multiple oceanic anoxic events during Permian–Triassic



- transition and the link with end-Permian extinction and recovery. *Earth Planet Sci Lett* 353–354:12–21
- Song H, Wignall PB, Chu D, Tong J, Sun Y, Song H, He W, Tian L (2014) Anoxia/high temperature double whammy during the Permian–Triassic marine crisis and its aftermath. *Sci Rep* 4:4132
- Tan X, Luo B, Jiang X, Liu H, Li L, Zhang B, Zou J, Zhao C (2012) Controlling effect of basement fault on Changxing formation reef in Sichuan Basin. *Geol Rev* 58(2):277–284 **(in Chinese with English abstract)**
- Tang H, Tan X, Liu H, Zhou Y, Li L, Ding X, Tang Q, Zou J (2014) Genesis and dolomitization of “Khali” powder crystal dolomite in Triassic Jialingjiang Formation, Moxi gas field, central Sichuan Basin, SW China. *Pet Explor Dev* 41(4):553–562
- Twitchett RJ, Krystyn L, Baud A, Wheeley JR, Richoz S (2004) Rapid marine recovery after the end-Permian mass-extinction event in the absence of marine anoxia. *Geology* 32(9):805
- Vennin E, Olivier N, Brayard A, Bour I, Thomazo C, Escarguel G, Fara E, Bylund KG, Jenks JF, Stephen DA, Hofmann R, Pufahl P (2015) Microbial deposits in the aftermath of the end-Permian mass extinction: a diverging case from the Mineral Mountains (Utah, USA). *Sedimentology* 62(3):753–792
- Wang BJ (1989) The Sichuan Hydrocarbon Province: petroleum geology of China, vol 10. Petroleum Industry Press, Beijing **(in Chinese)**
- Wang Y, Tong J, Wang J, Zhou X (2005) Calcimicrobialite after end-Permian mass extinction in South China and its palaeoenvironmental significance. *Chin Sci Bull* 50(7):665–671
- Wang R, Jiao Y, Wu L, Rong H, Li R, Wang S, Yang S (2009) Reef-forming model of Honghua reefs of the Upper Permian Changxing Formation in Kaixian, Chongqing. *J Palaeogeogr* 11(2):157–166 **(in Chinese with English abstract)**
- Wang L, Wignall PB, Wang Y, Jiang H, Sun Y, Li G, Yuan J, Lai X (2016) Depositional conditions and revised age of the Permian–Triassic microbialites at Gaohua section, Cili County (Hunan Province, South China). *Palaeogeogr Palaeoclimatol Palaeoecol* 443:156–166
- Wheeley J, Twitchett R (2005) Palaeoecological significance of a new Griesbachian (Early Triassic) gastropod assemblage from Oman. *Lethaia* 38(1):37–45
- Wignall PB, Bond DPG, Sun Y, Grasby SE, Beauchamp B, Joachimski MM, Blomeier DPG (2015) Ultra-shallow-marine anoxia in an Early Triassic shallow-marine clastic ramp (Spitsbergen) and the suppression of benthic radiation. *Geol Mag* 153(2):1–16
- Woods AD (2014) Assessing Early Triassic paleoceanographic conditions via unusual sedimentary fabrics and features. *Earth Sci Rev* 137:6–18
- Wu Y, Jiang H, Yang W, Fan J (2007) Microbialite of anoxic condition from Permian–Triassic transition in Guizhou, China. *Sci China Ser D Earth Sci* 50(7):1040–1051
- Wu YS, Yu GL, Li RH, Song LR, Jiang HX, Riding R, Liu LJ, Liu DY, Zhao R (2014) Cyanobacterial fossils from 252 Ma old microbialites and their environmental significance. *Sci Rep* 4:3820
- Wu YS, Yu GL, Jiang HX, Liu LJ, Zhao R (2016) Role and lifestyle of calcified cyanobacteria (Stanieria) in Permian–Triassic boundary microbialites. *Palaeogeogr Palaeoclimatol Palaeoecol* 448:39–47
- Xiang L, Schoepfer SD, Zhang H, DX Yuan, CQ Cao, QF Zheng, Henderson CM, SZ Shen (2016) Oceanic redox evolution across the end-Permian mass extinction at Shangsi, South China. *Palaeogeogr Palaeoclimatol Palaeoecol* 448:59–71
- Xie X, Li H, Xiong X, Huang J, Yan J, Qin J, Tenger Li W (2008) Main controlling factors of organic matter richness in a Permian section of Guangyuan, Northeast Sichuan. *J China Univ Geosci* 19(5):507–517
- Yang H, Chen ZQ, Wang Y, Tong J, Song H, Chen J (2011) Composition and structure of microbialite ecosystems following the end-Permian mass extinction in South China. *Palaeogeogr Palaeoclimatol Palaeoecol* 308(1–2):111–128
- Yao D, Yao W, Li C, Yuan M (2002) Geological map of Sichuan & Chongqing Province. In: Ma L (ed) *Geological Atlas of China*. Geology Press, Beijing, pp 277–284
- Zhao X, Tong J, Yao H, Zhang K, Zq C (2008) Anachronistic facies in the Lower Triassic of South China and their implications to the ecosystems during the recovery time. *Sci China Ser D Earth Sci* 51(11):1646–1657
- Zhong N, Lu S, Huang Z, Zhang Y, Xue H, Pan C (2004) TOC changes in the process of thermal evolution of source rock and its controls. *Sci China Earth Sci* 47(S2):141–149